View metadata, citation and similar papers at core.ac.uk

brought to you by CORE

provided by Clemson University: TigerPrints

Clemson University
TigerPrints

All Theses | Theses

12-2012

Ultraluminous X-ray Sources in Andromeda Galaxy: Two Recent Discoveries and their Implications

Amanpreet Kaur
Clemson University, akaur@clemson.edu

Follow this and additional works at: https://tigerprints.clemson.edu/all_theses

 Part of the Physics Commons

Recommended Citation
Kaur, Amanpreet, "Ultraluminous X-ray Sources in Andromeda Galaxy: Two Recent Discoveries and their Implications" (2012). *All Theses*. 1565.
https://tigerprints.clemson.edu/all_theses/1565

This Thesis is brought to you for free and open access by the Theses at TigerPrints. It has been accepted for inclusion in All Theses by an authorized administrator of TigerPrints. For more information, please contact kokeefe@clemson.edu.

Ultraluminous X-Ray Sources in the Andromeda Galaxy: Two Recent Discoveries and their Implications

---

A Dissertation
Presented to
the Graduate School of
Clemson University

In Partial Fulfillment
of the Requirements for the Degree
Master of Science
Physics

---

by
Amanpreet Kaur
December 2012

Accepted by:
Dr. Dieter H. Hartmann, Committee Chair
Dr. Mark D. Leising
Dr. Sean D. Brittian

Abstract

Ultraluminous X-ray sources are believed to be associated with X-ray binaries, in which an accreting black hole generates X-ray luminosities in excess of 10^{39} erg/s. The nature of the companion star and the underlying physics of the accretion process is not yet established with certainty. In particular, whether or not the accretion is super/sub Eddington is an open question, as is the mass of the companion star. We discuss the first two ULXs recently discovered in M31 and investigate the nature of their underlying sources. We present the X-ray observations for ULX-1 in detail and discuss its implications for its accretor. We also considered the positions of both ULX sources in the context of their hypothetical association with either High Mass X-ray Binaries and Low Mass X-ray Binaries. We construct a simple disk plus bulge model to test their association with starlight and use IR images from Spitzer to investigate their possible link to star formation. We find that the position of these two sources more strongly supports scenarios in which the companion is a high mass star. Using the data obtained with XMM-Newton, Swift and Chandra, we infer that the underlying source for ULX-1 is a 13 $M_{\odot}$ black hole under the assumption that it is non-spinning. The combined study of X-ray properties and the spatial distribution presented in this thesis argue in favor of stellar mass black holes accreting at near Eddington rates from high mass companions.

Dedication

To my Grandpa...

Acknowledgments

I am grateful to my advisor Dr. Dieter Hartmann for his guidance, support and patience. I thank my committee, Dr. Mark Leising and Dr. Sean Brittain for their suggestions that improved my thesis. I owe much gratitude to my family for being supportive throughout, and friends at Clemson, who made me feel at home in a foreign place.

This work utilized data obtained with XMM-Newton, Swift and Chandra under the nova monitoring program at MPE, Germany. I also thank the "Nova monitoring program in M31" team for providing me an opportunity to work on this project. In particular, I am grateful for the many valuable contributions from Dr. Martin Henze, which enabled me to complete this project. Special thanks to Ginger Bryngelson for her expert advice on IDL.

Table of Contents

List of Tables

List of Figures

Chapter 1

Introduction

Ultraluminous X-ray sources are very bright X-ray non-nuclear sources, with typical X-ray luminosities, $L_X = 10^{39-41}$ erg/s, which is 100-1000 times the luminosity of an ordinary X-ray source in a galaxy. These are believed to be associated with X-ray binaries, in which a black hole accretes matter from its companion. The mass of the underlying black hole can be estimated, assuming an isotropic emission from the accretion disk under hydrostatic equilibrium, the maximum luminosity from this system cannot exceed the Eddington luminosity,

$$L_{Edd} = 1.3 \times 10^{38} \frac{M}{M_\odot}$$

This implies that the underlying source for these systems, must be $>$ 10 - 1000 $M_\odot$ accreting black hole. There are few problems with this approach, one being the black holes with masses of the order of 100-1000 $M_\odot$, also called the 'Intermediate Mass Black Holes' (IMBHs), have not been observed yet. Other prominent problem is that the observed luminosity exceeds the Eddington limit of a 10 $M_\odot$ stellar black hole, which would require a super-Eddington accretion on to the underlying black hole

(Begelman, 2002). Moreover, study of ULX systems could fill in the gap between the Stellar Mass Black Holes, ($M < 80\ M_{\odot}$ (Belczynski et al., 2010)) and the Supermassive Black holes ($10^{6-9}\ M_{\odot}$ (Banerji et al., 2012)). To understand their true nature, various studies of ULXs are being conducted since law few decades. But due to their rare occurrence, this is a very challenging task.

1.1 History

The very first observations of ULXs were made with *Einstein Satellite* in 1980s (Fabbiano, 1989). These were observed as very bright X-ray sources(ULXs) near centers of various galaxies. But, due to the low spatial resolution of the Imaging Proportional Counter instrument (FWHM $\sim$ 1') on *Einstein*, it was difficult to separate these sources from the nucleus of galaxies. These observations lead to various speculations about the nature of these X-ray sources e.g. AGNs with a low accretion rate, a massive stellar mass black hole accreting at high rate, very luminous X-ray Supernovae etc. For review, see Fabbiano (1989). With the launch of ROSAT satellite in 1990, incorporated with a much higher resolution instrument (High Resolution Imager, PSF = 10"), and many more observations of ULXs were conducted and the case turned out to be such that these sources were not associated with AGNs. e.g. surveys of nearby galaxies by Colbert et al. (1999), Colbert and Ptak (2002) using ROSAT-HRI.

The observations mainly in X-ray and optical regime allows us to study the nature of the X-ray binary systems associated with these ultra high luminous objects. Listed below are some of the implications of studies of ULXs in these two regimes.

1.2 X-Ray Observations

The detection of a ULX is obviously confirmed in X-ray regime. As explained earlier, the very first X-ray observations of ULXs were conducted with *Einstein*, followed by ROSAT-HRI. There have been a lot more detections of ULXs after the introduction of the new era of X-ray astronomy with XMM-Newton, Swift and Chandra telescopes. In general, the data obtained with these telescopes is analyzed for the estimation of various parameters for the accretion disk and the underlying black hole. A variety of spectral models have been introduced (discussed in chapter 3.) to analyze the X-ray spectra (2-10 keV). e.g. Walton et al. (2010), Swartz et al. (2004), Winter et al. (2006), Sutton et al. (2012). Analysis of obtained data confirm a stellar mass black hole as the underlying source in most of the cases, but there exist few examples, which reveal the underlying sources as IMBHs e.g. Colbert and Ptak (2002), Miller et al. (2004). Recently, Webb et al. (2012) claimed to confirm the first observation of an IMBH based on multi-epoch observations and analysis.

1.3 Optical Observations

In X-ray binary systems associated with ULXs, the optical counterpart studies often reveal a massive O/Be type star as the companion. See Nooraee et al. (2012) for the optical counterpart studies of the first ULX observed in M31. These observations imply High Mass X-ray Binaries (HMXBs) as the underlying sources for the ULXs. In these systems, the companion is usually a massive Be/O star, with very strong winds, which are captured by the primary component i.e. the compact black hole (vanParadijs,J. and McClintock,J.E., 1995).

A recent discovery of ULX in M83 did not agree with the ULX-HMXB association

hypothesis, rather the studies revealed a Low Mass X-ray Binary (LMXB) as the companion for this ULX (Soria et al., 2012). Although during the observations, the authors recovered a blue optical counterpart associated with this ULX, but prior to this ULX discovery, no massive/blue stars were found in that region. Rather, this region in M83 is dominated by red stars. The face-on galaxy, M83 has very well established population studies, which made these authors claim the LMXB association with ULXs rather than HMXB association. They proposed that the X-ray irradiation during the ULX outburst could be responsible for brightening the binary systems, as a whole, which would lead to a higher observed flux.

The main properties of HMXBs and LMXBs are highlighted in the table below.

Low Mass X-ray Binaries	**High Mass X-ray Binaries**
1) Late type or degenerate star	1) Massive early type O/Be star
< 1.0 $M_\odot$ as companion	> 10 $M_\odot$ as companion
2) Long orbital period	2) Short orbital period
1 - 365 days	$\sim$ a few days
3) Distributed over the galactic disk	3)Distributed along the galactic plane
4) Young populations, $< 10^7$ yrs	4) Old population, $> 10^9$ yrs
5) Mass accretion via strong winds	5) Mass accretion via Roche Lobe overflow

Moreover, ULXs are followed up in radio regime, as well (e.g.(Kaaret, 2002), (Miller et al., 2005), (Kaaret, 2002)) to correlate with X-ray observations and optical studies to constrain the nature of associated black holes. A steady state emission from an IMBH in hard state or a relativistically beamed jet in the direction of observer are the two main scenarios tested with radio observations.

Based on these observational parameters, a few theoretical models have been developed to explain the nature of the main compact source associated with ULX phenomenon, which are discussed in the next chapter.

Chapter 2

Theoretical Source Models for ULX Systems

In this chapter, we discuss the various theoretical models suggested to explain very high luminosities observed in Ultraluminous X-ray sources. Since their discovery in 1980s by *Einstein Observatory* (Fabbiano, 1989), the three main models that were developed are explained as follows:

Based on their observed properties, as discussed in the introduction, it appears natural to hypothesize that the underlying source population involves accreting black holes. In that case, the luminosity scale is set by the Eddington luminosity, leading us to consider two major theoretical approaches: Super-Eddington accretion onto Stellar Mass black holes and Sub-Eddington accretion onto Intermediate mass black holes. The former class involves black holes resulting from standard stellar evolution, while the latter involves a thus far unobserved mass range of black holes (>100 $M_{\odot}$). We also briefly discuss the geometric beaming as another theoretical aspect for the observed high luminosities.

2.1 Super-Eddington Accretion onto a Stellar Mass Black Hole

Begelman (2002) proposed that Super-Eddington accretion onto a stellar mass black hole can lead to the birth of an ultraluminous X-ray source. He argues that in a magnetized and radiation pressure dominated atmosphere, a non-linear photon-bubble instability (Gammie, 1998) causes significant inhomogeneities at much smaller scale than the radiation pressure scale height. In these circumstances, a magnetohydrodynamical wave propagating in a direction perpendicular to the direction of the energy flow, causes variations in the density of the gas.

Radiation 'leaks' through the low density regions in these systems into the interstellar medium. These inhomogeneities exhibit nonlinear wave patterns, which follow from a gas cycle between low density and high density regions as explained by Begelman (2001). The author suggested non-linear plane wave solutions, in a steady state, in which radiation pressure and magnetic tension forces are dynamically coupled. The main point in the context of ULXs is that the total flux observed from such an atmosphere can exceed the Eddington limit without dynamically disrupting the atmosphere. In other words, the classical Eddington limit for a stable accreting compact star can be circumvented in atmospheres with significant inhomogeneities.

The accreted matter in a ULX system is likely donated by a companion star in a binary system. Thus the acrretion flow is not spherically symmetric, but rather flows through an accretion disk. black hole . Accretion disks around the Stellar Mass Black Holes (StMBH) could exhibit similar conditions as the atmospheres discussed above. This would allow luminosities observed from ULXs to be attributed to disks that accrete at Super-Eddington rates.Begelman (2002) considered a model of a thin

Keplerian disk accreting at a rate,$\dot{M}$, with an inhomogeneous radiation dominated atmosphere and concluded that the maximum possible luminosity from such a disk is

$$\frac{L_{max}}{L_{Edd}} > 30\ \xi_{-1}^{4/5}\alpha_{-2}\left(\frac{M}{10}\right)^{1/5}\epsilon_{0.1}\left(\frac{x_{ISCO}}{6}\right)^{1/2},$$

$$\dot{m_{in,max}} \sim (x_{in}/x_{inhom})^{1/2}$$

where x_{inhom} is such that at a distance greater than x_{inhom} from the center of the disk, inhomogeneities would be ineffective, ϵ is accretion efficiency (typically, 10%), ξ reflects the efficiency by which the bubbles boost the luminosity. The additional parameter, α in this equation describes the viscosity of the disk(this model uses and α disk with typical value 1%) Typical value of ξ for these systems lies between $0.01 - 0.1$ and M is the mass of the black hole in the system.

Based on this equation, the author justified that the accretion disks around stellar mass black holes can produce luminosities as much as 10 -100 times the Eddington limit, without driving a significant mass loss. However, beyond this luminosity, the instabilities in the magnetic field would result in a disruption of the disk. The observed luminosities of ULX sources, when interpreted as accretion onto stellar mass black holes with M $\sim$ 10-20 $M_{\odot}$ are compatible with this class of models. However, we have no observational diagnostic that would allow us to see its possibility.

2.2 Intermediate Mass Black Holes

The previous scenario solved the problem of high luminosities from the more or less stable accretion environment on stellar mass black holes.One could also consider Eddington or even sub-Eddington accretion onto much more massive black holes. The

observed luminosities, is interpreted as Eddington luminosities that imply black hole masses of the order of 100 - 1000 $M_{\odot}$ for ULX sources. There is nothing wrong with this approach, except that one now faces a question,ofhow these black holes were created in the first place. Combining a standard initial mass function and stellar evolution theory, one can expect a maximum mass of 80 M$\odot$ (Belczynski et al., 2010) for remnants of stellar evolution is. It is thus not clear, where black holes in this mass range should have come from. This hypothetical class of black holes, referred to as IMBHs are in between those masses emerging from stellar evolution and the much higher masses found in the cores of the galaxies. The latter class covered a mass spectrum from 10^6 to 10^9 and beyond. The ULXs are not coincident with the galactic centers, so the SMBH class is not a viable model. The existence of these IMBHs have not been established, ambiguously. Infact, some ULX sources have been used to argue in support of this class. Therefore, we now consider this model in more detail:

The high signal to noise X-ray spectral analysis of ULXs in various galaxies provided a strong indication towards the existence of these black holes with intermediate masses e.g. spectra of ULX in NGC1313 Miller et al. (2004) was fitted with a power law and multicolored disk, with inner temperature of the order of 0.1keV. X-ray binaries, in general, show the same characteristics but with ahigher temperature $\sim$ 1-2keV. For the fixed accretion rate, the temperature is proportional to $M^{-0.25}$, which implies that the binary system contains a rather massive black hole. The existence of black holes with intermediate mass had been suspected by various groups more than 3 decades ago, e.g. Marchant and Shapiro (1980), Fabian,A.C. and Ward,M.J. (1993), Colbert et al. (1999), Zwart et al. (2004), Miller et al. (2004), Fabian et al. (2004), Dewangan et al. (2004), Roberts et al. (2005), Sutton et al. (2012) and probably others, though there had been no confirmed observational evidence. What was

lacking was a detailed observational support for this identification for this scenario. Recently, Webb et al. (2012) claimed a strong observational support for this assertion when adding radio data to the X-ray signature of ESO 243-49. This source is actually identified as hyperluminous X-ray source, HLX-1,with $L_X > 10^{41}$ erg/s). The authors identified a correlation between radio and X-ray emission which suggests that it is an IMBH. It is thus conceivable that ULX sources are associated with stellar mass black holes, exhibiting super-Eddington luminosities, while HLXs are indeed IMBHs radiating at sub-Eddington luminosity. The progenitor systems of ULXs sources would thus be massive stars, while the progentiors of HLXs remained to be explained.

The absence of observational evidence as well as the theoretical complexities for the formation of these black holes with intermediate mass pose significant challenges in this field. Below we discuss various paths suggested for the formations of IMBHs.

2.2.1 Formation from Population III Stellar Evolution

Fryer (1999) suggested that the black hole remnants of population III stars are expected to be more massive as compared to the stellar mass black holes, as a result of the limited mass loss due to their low metallicity. The authors argued that if a star had mass greater than 260 $M_\odot$, nuclear burning would not be able to generate an explosion. Consequently, it would collapse directly into a black hole of mass larger than half of the mass of the star itself. Colbert et al. (1999) suggested the existence of these black holes based on the spectral modeling of ROSAT HRI data of 21 face-on spiral and elliptical galaxies. The spectral analysis lead the authors to estimate the black hole masses for the observed ULXs in M33, NGC1313 and NGC5408 to be greater than 100 $M_\odot$. But the absence of observational evidence of these objects brought up

a question of theory of the formation of these black holes with intermediate masses. Thus, IMBH formation can be expected following this mechanism.However, the problem with this approach is the evidence of a star with mass $\sim 260\ M_{\odot}$. Madau and Rees (2001) suggested a possibility of big population of IMBHs in a galaxy (10^3-10^4), based on the above mentioned assumption of population III stars being rather massive.

Based on the above scenario, Miller and Colbert (2004) calculated that the expected number of ULXs in a galaxy as follows:

$$N_{ULX} = n_{IMBH} N_{cluster} \sigma_{cluster} v_{rel} T$$

n_{IMBH} = number density of IMBH

$N_{cluster}$ = number of super star clusters

$\sigma_{cluster}$ = cross-section of interaction of an IMBH with a cluster

v_{rel} = relative velocity at infinity of the IMBH

T= Lifetime of the cluster

But the basic constraint on this theory is absence of an observation evidence of population III stars, which leads to a possibility of high uncertainty in mass range of these old stars.

2.2.2 Formation in Dense Star Clusters

The study of stellar mergers by Quinlan and Shapiro (1990) due the core collapse process yielded that runaway collisions in very dense clusters ($\rho > 10^6$ $M_{\odot}pc^{-3}$) lead to the formation of very massive black holes, the so called IMBHs. Zwart et al. (2004) demonstrated this by performing numerical simulations of the evolution and

motion of the stars within the clusters. They discovered that if stars are allowed to merge with each other during the evolution process via runaway collision, the dynamical friction leads to the formation of massive stars, which sink rapidly to the center of the cluster and finally collapsed to form intermediate mass black holes, which can be observed as ultraluminous X-ray sources.

2.2.3 Formation by accretion onto Stellar Mass Black Holes

Another possible path for the formation of these IMBHs is the substantial growth in mass of a stellar mass black hole by accretion from the interstellar medium. However, Miller and Colbert (2004) ruled out this possibility because the stellar mass black hole would not be able to accrete sufficient mass from the interstellar medium in a Hubble time.

2.2.4 Formation in Globular Clusters

Miller and Hamilton (2002) et al. explained that the core collapse process in globular clusters is generally halted by binary heating, therefore it is highly improbable to explain the existence/formation of an IMBH in such a system. But this is not always true, provided a very massive star undergoes core collapse on a timescale much less than the core collapse for the cluster itself (Zwart et al., 2001). These authors developed a N-body simulations to demonstrate that a runaway merger in a globular cluster could undergo core collapse process much faster than the core collapse of the cluster itself, provided that this collapse occurs at a timescale much faster than their main-sequence lifetime.

2.3 Anisotropy

One out of the three models put forward for the sources responsible for the generation of the high X-ray luminosity observed from the ultraluminous X-ray sources is anisotropic emission from the accretion disk.

King et al. (2001) considered a model in which it is assumed that the X-ray emission from X-rays is significantly beamed. The authors suggested that ULXs might be a short thermal-timescale mass transfer phase for compact intermediate or high-mass X-ray binaries during their evolution. Assuming a beamed model with beaming factor, b = $\Omega/4\pi$, where Ω is the solid angle of emission.if L_{sph} is the luminosity for an isotropic emission, then the net luminosity due to beaming effects is

$$L = b\ L_{sph} = 10^{40} b L_{40}$$

erg/s

and

$$L_{40} = \frac{L_{sph}}{10^{40}}$$

This implies the mass of underlying black hole accreting within Eddington limit is

$$M_{BH} \geq 10^2 b\ L_{40} M_{\odot}$$

and hence for b $\sim 0.1 - 0.01$, the calculated M_{BH} reduces to the value for a typical observed X-ray binary system. But the uncertainty for this model is whether beaming is a common effect observed in X-ray binaries or not.

2.4 Summary

The rare occurrence of ULXs per galaxy has to date resulted in a total sample of ~ 475 (Walton et al., 2010) in nearby galaxies . The bulk of these sources reside in nearby host galaxies, with cz < 1000 km s^{-1}. It is definitely the case that ULXs are not associated with the centroid of the galaxy, arguing against the involvement of the SMBHs known to reside in almost all the galaxies. From studies of host galaxies, it appears that ULXs trace star formation patterns in star forming galaxies. This association suggests a link between HXMBs and ULXs. However, not all ULXs are associated with star forming structures and in a few cases are found in elliptical galaxies (Walton et al., 2010). These latter findings suggest that some, perhaps most ULXs trace an old population of stars and would thus be associated with LXMB population. Later chapters explore these alternatives for the nearby galaxy M31 with two known ULXs.

Chapter 3

Spectral Models of Underlying Sources

The spectra obtained from a X-ray binary system is analyzed employing different spectral models, developed by various astrophysicists over the years, with different assumptions regarding the geometry of the accretion disk and the nature of the underlying sources. The most common models utilized for the spectral analysis of ultraluminous X-ray sources are discussed below.

3.1 Thermal (Soft) and Non-Thermal (Hard) Model

3.1.1 Multicolored Disk model: Thermal Component

Multicolored disk model (MCD) is commonly employed to fit X-ray spectra for X-ray binaries. Proposed by Shakura,N.I. and Sunyaev,R.A. (1973), Mitsuda,K. et al. (1984), this model is composed of a geometrically thin accretion disk, which is assumed to be a blackbody with temperature varying with distance from the center of the black hole. The flux obtained from this model is:

$$f(E) = \frac{cos\theta}{R^2} \int_{r_{in}}^{r_{out}} 2\pi r B_E(T) dr$$

and for a thin disk

$$T \propto r^{-3/4}$$

B_E(T) is Planck function at energy E, θ is the angle of the disk axis with respect to the line of sight, and R is the distance to the source.

Under the same assumptions of a geometrically and optically thick accretion disk, Makishima et al. (2000) applied the following relationship between mass of the black hole and the innermost temperature of the accretion disk around it, to ULX spectra:

$$kT_{in} \approx 1.2 \left(\frac{\xi}{0.41}\right)^{1/2} \left(\frac{\kappa}{1.7}\right) \alpha^{-1/2} \left(\frac{\dot{M}}{\dot{M}_E}\right)^{1/4} \left(\frac{M}{10M_\odot}\right)^{-1/4} keV$$

$\xi \approx 0.41$ and it takes into account that the maximum temperature occurs at a radius larger than the stable innermost radius of the disk. $\alpha = c^2 \frac{R_{in}}{6GM}$ accounts for the rotating (*Kerr*) or non-rotating (*Schwarzchild)* black hole. For a stationary black hole, its value is unity whereas for rotating systems it is less than unity and for maximum spin its value is 1/6.

But these implications of X-ray spectral analysis from this model fitting are not always physically right. There are approximately 10 ULX's spectra, which when fitted with this model, derives the temperature of the inner disk greater than 1 keV,

ruling out the possibility of an IMBH accreting at sub-Eddington limit. The possible explanation for this "high temperature" problem by Makishima et al. (2000) are variation of ξ and σ values from "normal", or if the underlying black hole is a Kerr black hole i.e. $r_{in} < 3$ GM/c^2, then the observed higher temperature can be justified at even smaller values of radius of inner most stable orbit.

3.1.2 Powerlaw: Non-Thermal Component

Power law spectrum as a result of highly relativistic electrons accelerating in presence of magnetic field lines i.e. synchrotron radiation. The flux received from this component can be calculated by the simple mathematical power law, with photon index, α and normalization constant, K :

$$F(E) = KE^{-\alpha}$$

and

$$F(E) = KE^{-\alpha_1} for E < E_{break}$$

$$= KE_{break}^{\alpha_2-\alpha_1} E^{-\alpha_2}$$

is the broken powerlaw.

Most of the spectra of ULXs are fitted with combination of powerlaw and MCD models to deduce various parameters of the system such as temperature, mass of the black hole, accretion rate, inclination of the disk etc. Over the last few years, various other physically motivated models have been developed to analyze ULX spectra, discussed as follows:

3.2 Slim Disk Model

Abramowicz et al. (1988) discussed the slim disk model for accretion theory, in which

all the gravitational energy released is not only converted into thermal radiation but a significant part of it is carried away through the radial advection. In this scenario, the accretion disk is geometrically thick such that the observed luminosity can exceed the Eddington limit, without disruption of the disk, itself. Hence, the temperature gradient changes as $T \propto r^p$, where p is the disk free parameter, DISKPBB in `XSPEC`. Although, in a standard disk model, p = 3/4, whereas in 'slim' disk model, the value of p is not fixed

Mathematically, Ebisawa,Ken et al. (2003) derived the luminosity from the flux observed from a disk of radius r and half-thickness, h.

$$F(r) \sim \frac{c\,GM}{\kappa r^2}\frac{h}{r}$$

which implies $L_{disk} = 2\int_{r_{in}}^{r_{out}} 2\pi r F(r) dr$

or

$$L_{disk} \approx L_{Edd}\left(\frac{h}{r}\right) ln\left(\frac{r_{out}}{r_{in}}\right)$$

In general, $r_{out}/r_{in} \approx 10.$ and h/r ~ 1 for 'slim' disk model.

Gladstone et al. (2011) utilized this model for the analysis of some ULX spectra, but derived unrealistic values of temperature i.e. 6-13 keV. Therefore, these authors suggested an improvement in the slim disk model to investigate the physical importance of ULX spectra.

3.3 Comptonization Model

The existence of a turnover at high energies above 3 keV has been noticed through the study of high-quality ULX spectra by Stobbart et al. (2006). Gladstone et al. (2009) suggested that the comptonization due to the presence of an optically thick corona could artificially lower the temperatures obtained from the inner regions of the disk.

In general, Titarchuk (1994) `COMPTT` and Coppi,P.S. (2000) `EQPAIR` are two different compotonization models applied to black hole binaries. Gladstone et al. (2011) applied these models (instead of simple powerlaw) each, with a disk component for ULX spectral studies. The application of this model yielded an accretion disk with a cool, optically thick corona ($\tau \geq 6$), which is very different from the normal black hole states. For a standard black hole in a very high state, $\tau \leq 3$, which implies that ULXs correspond to an extremely high state for a standard black hole. The authors also suggested that the resultant cool disks can be attributed to the presence of IMBHs as well. Although, it was pointed out that the assumptionthat the inner regions of the disk are not affected by the presence of optically thick corona seems unphysical.

The flaws from the above model are taken into account and corrected by introduction of an **energetically coupled disk and corona model** referred as DKBBFTH (Done and Kubota, 2006), which assumes the increased accretion rate with more energy and matter fed to corona.

3.4 Reflection Model

Ross and Fabian (2005) proposed a model for accretion disks in compact binary systems based on X-ray irradiation. According to this model, the soft X-ray component (often thought as an outcome of the accretion disk) is a consequence of blurred reflection above the disk due to the backscattering and fluorescence of X-rays. Therefore, the inner regions of an accretion disk cannot be observed, and thereby derivation of inner temperature of the disk, mass of the black hole and other parameters cannot be calculated by a simple multicolored disk model.

The authors introduced this model called REFLEXION in XSPEC. Caballero-García and Fabian (2010) analyzed spectra of ULXs in NGC1313, M82, NGC5408, HOLM IX employing this model in conjunction with powerlaw and concluded that the underlying sources in ULXs might be fast spinning black holes and the reflection due to X-ray irradiation just above the accretion flow could be responsible for soft excess observed in the spectra.

Though a variety of models developed over the years have been used to perform the spectral analysis of ULXs, but most of these complicated models have flaws of different nature as discussed above, therefore they provide no better insight to the understanding of the true nature of these sources. Hence, the combination of a simple power law with a multicolored disk component is still a favorable model for spectral analysis of ULXs.

Chapter 4

Observations and Analysis of ULX-1 in M31

4.1 ULXs in M31

About ~ 475 ULXs in nearby galaxies have been discovered in last few decades, starting with the very first observations recorded during *Einstein Era* in 1980s (Fabbiano, 1989). In our nearest neighborhood i.e. in Andromeda galaxy, two ULXs have been discovered recently. On December 17 2009, the first ULX (CXOM31 J004253.1 +411422) was discovered by Chandra through our nova monitoring program[1] for resolving super-soft source states of optical novae in the central area of M31 with XMM-*Newton* and *Chandra* HRC−I (Henze,M. et al., 2009). On January 26, 2012, another ULX named XMMU J004243.6+412519 (ULX-2 from now on) was reported by Henze,M. et al. (2012) within the same monitoring program. In this chapter the X-ray spectral analysis of the first ULX, CXOM31 J004253.1 +411422 (ULX-1 from

[0]**This chapter is based on the article published as Kaur et al. (2012)**

[1]http://www.mpe.mpg.de/ m31novae/xray/ao10/index.php

now on) is discussed in detail.

4.2 Observations and Analysis

The position of ULX-1 in M31 was determined to be R.A. (J2000) = 00:42:53.15 and Dec (J2000) = +41:14:22.9, using the catalog of X-ray sources in M31 assembled by Kaaret (2002). The source position with respect to the center of M31 is shown in Figure 1, obtained with XMM-Newton. An optical counterpart with m(F435W)=23.8 mag was identified in HST observations by Garcia,M. et al. (2010). The data was first obtained with *Chandra* HRC-I and then followed up with XMM-Newton and *Swift*-`XRT` till February 26, 2012. See the details in Table 1.

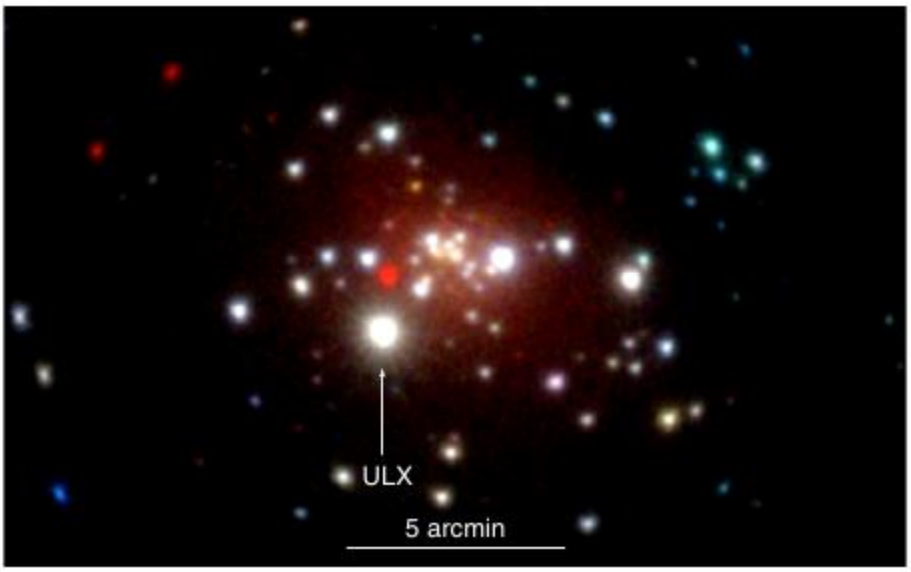

Figure 4.1 XMM-Newton EPIC image of the central part of M31 produced by combining pn, MOS1 and MOS2 data from all 5 observations. Red, green and blue show the $(0.2 - 1.0)$ keV, $(1.0 - 2.0)$ keV) and $(2.0 - 12.0)$ keV energy bands, respectively.

The data obtained from Chandra was analyzed using `CIAO` (Chandra Interat-

ice Analysis of Observations;)[2] and level 2 event files were analyzed to obtained count rates. For XMM-Newton data, an adapted version of XMMSAS[3] tool emldetect was used to estimate background-corrected and exposure-corrected fluxes and count rates. Swift-XRT data were analyzed with HEASOFT XIMAGE package (version 4.5.1) with the sosta (source statistics) command and count rates were determined. The XRT PSF was taken into account using command psf, and exposure maps were created with XRTexpomap command. The count rates obtained from all the data were converted to unabsorbed fluxes using XSPEC. Counts obtained from Swift-XRT and Chandra were converted to unabsorbed flux using energy conversion factors (ecfs). ecfs were computed using fakeit in XSPEC version 12.7.1[4] assuming the best fitting spectral model for the XMM-Newton observations at different epochs and using publicly available response files. For the Swift and Chandra observations obtained before and after the XMM-Newton observations, the first and last XMM-Newton sample was used to obtain ecf, respectively. The ecf values obtained are $\mathrm{ecf}_{HRC-I-1} = 6.3 \times 10^{10}$ cts cm^2 /erg and $\mathrm{ecf}_{HRC-I-2} = 7.7 \times 10^{10}$ cts cm^2 /erg. For Swift XRT, the $\mathrm{ecf}_{Swift} = 1.57 \times 10^{10}$ cts cm^2 /erg. Details can be found in Table 1.

The spectroscopic data were obtained with XMM-Newton using the European Photon Imaging Camera (EPIC), EPIC-pn , MOS1 and MOS2 CCD detectors are mounted on the three X-ray telescopes on XMM-Newton-Newton-Newton, as mentioned in Table 1. The XMMSAS version 10.0.0 was used to process the event files to generate images, response functions, spectra and light curves. The parameter setting for all three cameras, pn, MOS1 and MOS2 were as follows:

[2]http://cxc.harvard.edu/ciao/
[3]http://xmm.esa.int/sas/
[4]http://heasarc.gsfc.nasa.gov/xanadu/xspec/

Table 4.1 Observations Log

Telescope	Obs ID	Date (UT)	Exptime (ks)	Rate [a] (ct s^{-1})	L_{unabs} [b] (10^{39} erg s^{-1})
Chandra HRC-I	10885	2009−12−08.94	18.27	< 1.5e-03	0.002 [c]
Chandra HRC-I	10886	2009−12−17.90	18.34	3.300 ± 0.040	3.77 ± 0.04
Swift−XRT	00031518013	2009−12−22.04	3.6	0.660 ± 0.200	3.04 ± 0.20
Swift−XRT	00035336016	2009−12−23.05	4.2	0.720 ± 0.100	3.31 ± 0.10
Swift−XRT	00035336017	2009−12−24.04	4.8	0.620 ± 0.100	2.86 ± 0.10
Swift−XRT	00035336018	2009−12−25.05	5.2	0.600 ± 0.100	2.76 ± 0.10
Swift−XRT	00035336019	2009−12−26.26	5.0	0.560 ± 0.100	2.58 ± 0.10
Swift−XRT	00035336020	2009−12−27.07	5.0	0.580 ± 0.100	2.67 ± 0.10
XMM−Newton	0600660201	2009−12−28.53	16.86	6.447 ± 0.022 [d]	2.16 ± 0.07[f]
				1.810 ± 0.010 [e]	
				1.851 ± 0.010 [f]	
XMM−Newton	0600660301	2010−01−07.32	15.43	1.784 ± 0.012	1.49 ± 0.05 [g]
				1.105 ± 0.008	
				1.143 ± 0.008	
XMM−Newton	0600660401	2010−01−15.53	15.33	3.832 ± 0.017	1.16 ± 0.04[g]
				1.372 ± 0.009	
				1.402 ± 0.009	
XMM−Newton	0600660501	2010−01−25.11	17.83	3.042 ± 0.015	0.71 ± 0.03[g]
				0.846 ± 0.007	
				0.873 ± 0.007	
XMM−Newton	0600660601	2010−02−02.11	15.43	1.072 ± 0.009	0.65 ± 0.03[g]
				0.694 ± 0.006	
				0.687 ± 0.006	
Chandra HRC-I	10808	2010−02−15.86	17.12	0.547 ± 0.080	0.51 ± 0.08
Chandra HRC-I	11809	2010−02−26.27	18.42	0.490 ± 0.180	0.46 ± 0.18

[a]Count rate as observed from the source without rejecting pile-up pixels.
[b]Total unabsorbed luminosity from the source within (0.2−10 keV) energy band.
[c]3σ upper limit
[d]EPIC-pn
[e]MOS1
[f]MOS2
[g]Derived from the simultaneous fitting of EPIC−pn, MOS1 and MOS2 in XSPEC.

$FLAG = 0$; for bad pixels rejections

$PATTERN \leq 4$, for pn &

$PATTERN \leq 12$, for `MOS1` and `MOS2` ; for noise level reduction

Barycenter correction was performed using the `barycen` task in `XMMSAS`. The

light curves obtained were corrected for bad pixels, GTIs and vignetting using `epiclccorr`. An example of binned count rate in 100s intervals obtained from XMM-Newton `EPIC-pn` is shown in Fig. 2. The power density spectra was generated with the task called `powspec` in `FTOOLS` using the Fast Fourier Transform algorithm (`FFT`). The normalization for this process was chosen such that the white noise level expected from the data errors corresponds to a power of 2. The `XMMSAS` tool `epatplot` was used to check for pile-up for during spectrum extraction. The inner PSF part of the appropriate regions were excluded to avoid pile-up in the spectra. Response files were generated by using SAS tools `rmfgen` and `arfgen`. The spectral binning was constructed to attain 20 counts per bin to assure uniform statistics across the energy range. Bad pixels were ignored and energy channels from 0.2-10.0 keV were considered for spectral fitting using `XSPEC` version 12.6.0.

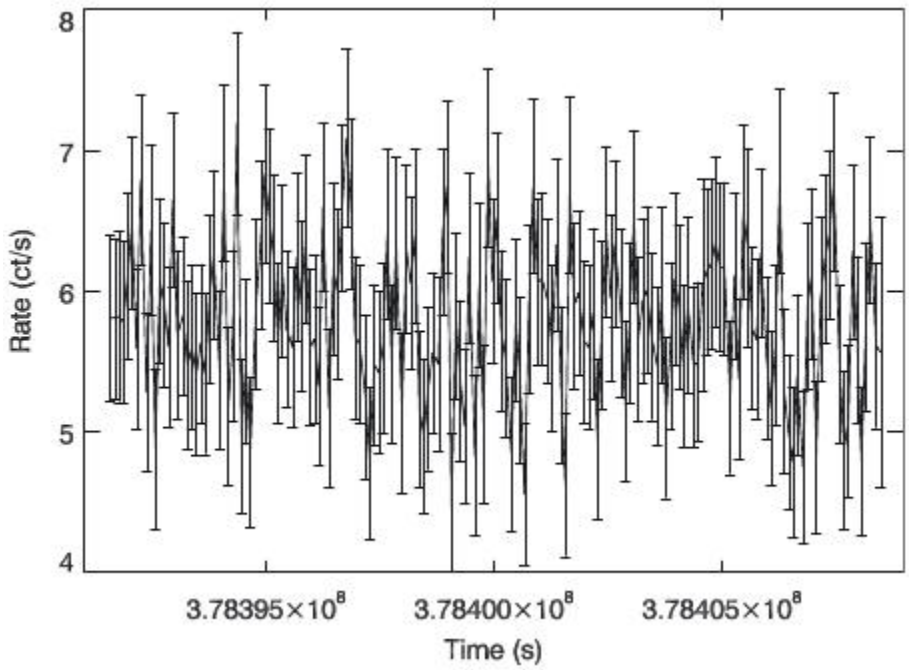

Figure 4.2 Light curve from XMM−Newton EPIC−pn for observation 0600220201 with time binning of 100 s in 0.2− 10 keV energy band.

4.3 Results

Broken powerlaw, powerlaw, multicolored blackbody or their combination thereof are the models, which are often employed for fitting a ULX spectra. We utilized these two models to fit our spectra obtained from XMM-Newton over different epochs. Broken powerlaw (`BKNPOWER` in `XSPEC`), when fit to data, resulted to χ^2 /degrees of freedom = 2953.96/1174, which was not a good fit. We achieved a better fitting using an alternative model that combined the powerlaw with multicolored disk (PO+DISKBB in `XSPEC`) to fit our spectra. The χ^2 values for the are listed in Table 2. The powerlaw component corresponds to a non-thermal and multicolored disk to a thermal component of a spectrum. The thermal component is associated with the accretion disk around a black hole as developed by Shakura,N.I. and Sunyaev,R.A. (1973), Mitsuda,K. et al. (1984) and Makishima et al. (2000). The extinction correction was applied to the spectrum due to the Milky way and the host galaxy for the object i.e. M31. For this process, extinction model Tuebingen-Boulder ISM absorption model (`TBABS`) (Wilms et al., 2000) was used in `XSPEC`. The hydrogen column density for Milky Way was fixed to 5.32×10^{20} cm^{-2} Dickey and Lockman (1990), whereas for M31, this parameter was included in the model as a free parameter. But the column density values derived did not account for the metallicity variation along our line of sight through the host galaxy, rather it assumed the same template as of Milky Way in terms of a standard cross-section per hydrogen atom. An example of this fitting procedure is illustrated in Fig. 3 for all the three cameras of XMM-Newton X-ray telescope. The decomposition of the X-ray spectrum into different model components is shows in Fig. 4.

From the derived parameters by spectral fitting, the resultant fluxes were

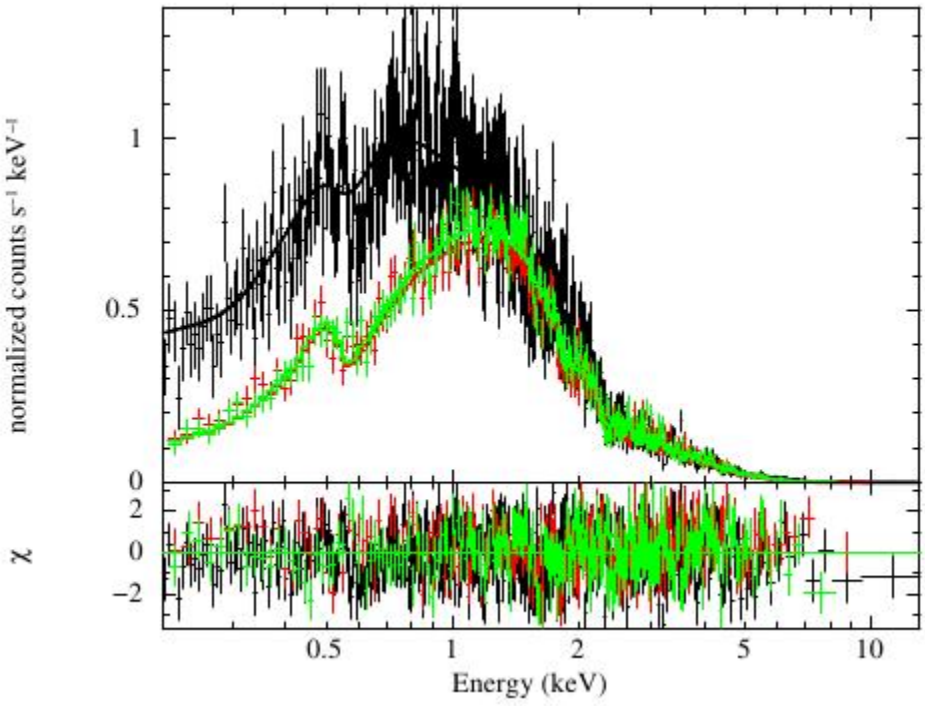

Figure 4.3 Combined powerlaw and multicolored blackbody fit to the joint set of data from EPIC−pn (black), MOS1 (green), MOS2 (red) with χ^2/ d.o.f. = 1318.87/1165 for the observation 0600660201 with XMM−Newton. The model parameters obtained from this spectral fit are presented in Table 2.

Table 4.2 The spectral parameters from the model fitting from XMM-Newton

OBSID	$N_{H,M\ 31}$ [5] (10^{20} cm^{-2})	kT [6] (keV)	Γ [7]	χ^2/d.o.f.	$R_{in}\sqrt{cos(i)}$ [8] (km)	L_{PO} [9] (10^{39} erg s^{-1})	L_{BB} [10] (10^{39} erg s^{-1})	L_{Total} [11] (10^{39} erg s^{-1})
0600660201	5.1 ± 1.1	1.070 ± 0.010	2.59 ± 0.16	1318.87/1165	52.90 ± 0.01	0.33 ± 0.07	0.94 ± 0.07	2.16 ± 0.07
0600660301	7.1 ± 1.2	0.993 ± 0.016	2.58 ± 0.13	963.62/991	58.89 ± 0.02	0.32 ± 0.05	0.71 ± 0.05	1.49 ± 0.05
0600660401	9.1 ± 1.2	0.913 ± 0.013	2.81 ± 0.14	1046.74/953	57.32 ± 0.02	0.33 ± 0.04	0.36 ± 0.04	1.16 ± 0.04
0600660501	5.3 ± 1.0	0.815 ± 0.014	2.51 ± 0.12	962.61/938	61.57 ± 0.02	0.23 ± 0.03	0.27 ± 0.03	0.71 ± 0.03
0600660601	6.5 ± 1.6	0.769 ± 0.013	2.70 ± 0.13	830.66/821	64.18 ± 0.03	0.16 ± 0.03	0.25 ± 0.03	0.65 ± 0.03

calculated, which were then converted to luminosity units with an assumption of M31 distance from the Sun equal 780 kpc (Holland, 1998), and isotropic emission. The resulting luminosity of the ULX were about 10^{39} erg/s, which places this X-ray binary into the category of Ultraluminous sources. Table 2. summarizes the derived values of different parameters obtained from model fitting and calculated luminosities. The luminosity due to thermal and non-thermal component each as a function of time

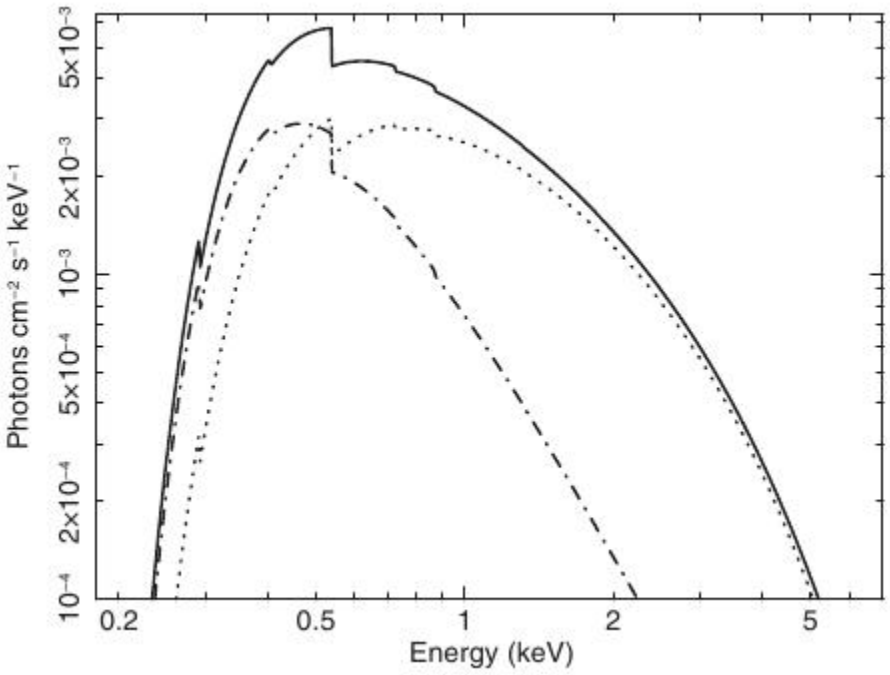

Figure 4.4 The theoretical model underlying the data fit (solid line) in Fig. 3 is shown in decomposition between the thermal (dash-dotted line)and the non−thermal (dotted line) component.

is shown in Fig. 5. The luminosity of this component during its peak (3.7×10^{39}) was higher than the total X-ray luminosity of M31 sampled by ROSAT (Supper et al., 1997) in the (0.1-2.4)keV band. Furthermore, this source is almost 10^3 times as bright as the other X-ray sources in M31. (Williams et al., 2006).

The first XMM-Newton observation corresponds to the brightest epoch of this ULX. X-ray spectrum fits analysis reveals that the most of the observed flux originated from the black body compoent during this observation, therefore, we estimate the mass of the black hole and the inclination utilizing the parameters from this data with the formalism given in the Makishima et al. (2000) under the assumption of a geometrically flat and optically thick accretion disk, these authors derived the equations mentioned in section 1.1 of chapter 3. We assumed the unabsorbed L_{bb}

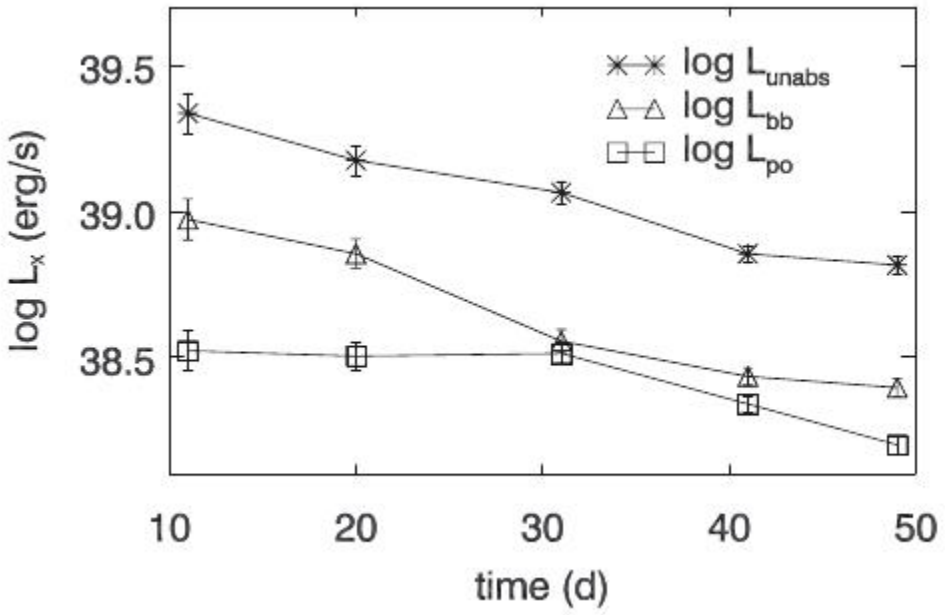

Figure 4.5 Temporal variation of the total unabsorbed luminosity (L_{unabs}) as per observations of XMM−Newton. The decomposition into the powerlaw (L_{po}) and blackbody component (L_{bb}) reveals a distinct evolutionary behavior of these two components. The time zero corresponds to *Chandra* HRC-I observation ID 10886 (see Table 1).

component (from Table 2. first XMM-Newton observation) = 1.6 × 10^{39} erg/s as the bolometric luminosity, because the major part of the total luminosity during this observation was a result of thermal component. From the two equations, we determined the mass and inclination angle, although significant uncertainties associated with the model parameters and fixed values of α, ξ, κ to 1, 0.41 and 1.7, respectively, are present. With all these assumptions and calculations, we find a mass of 13 $M_\odot$ for the underlying black hole in this binary system, with a statistical uncertainty of 4%. The inner radius calculated from this mass is R_{in}= 124 km. This implies, from the spectral fitting parameter, $R_{in}\sqrt{cos(i)}$, the inclination to be approximately 80°. This calculation is based on the assumption that the underlying source is a non-spinning black hole, which means that $\alpha = 1$, which could be an underestimation of the mass

of this black hole, if it is a rotating one. For a maximally spinning black hole, $\alpha = 1/6$. Therefore, the mass would be six times the mass of a non-spinning black hole and the underlying source would fall in the category of Intermediate mass black holes. The α value relies on the assumption that the inner edge of the accretion disk can be identified with the location of the innermost stable circular orbit (ISCO). However, determining the inner edge of a black hole accretion disk is a very complex matter e.g. Abramowicz et al. (2010)

We obtained the power spectra to search for the existence of periodicity for each of the spectra as mentioned in data analysis section, over a binning of 100s. The observed count rates show fluctuations within the range expected from counting statistics as shown in Fig 2. But the power spectra did not reveal any significant feature, i.e. there was no sign of quasi-periodic oscillations.

4.4 Discussion and Conclusions

The mass of the underlying black hole for this ULX implies a stellar mass black hole with all the assumptions (discussed above) taken into account. The calculated luminosity, too is consistent with the ULXs observed in nearby galaxies. The temperature and the photon index of M31 source falls in the center of observed distribution of ULXs by Winter et al. (2006), lending additional support to the nature of a ULX.

We analyzed the various properties of this ULX with a selected sample from the XMM-Newton archival study of ULXs by Winter et al. (2006) in 32 nearby galaxies with distance < 8Mpc and unabsorbed luminosities $> 10^{38}$ erg/s in the 0.3 -10 keV range of energy. Utilizing the properties of galactic black hole binaries, these

authors classified the ULXs into two categories, i.e. "low" state and "high" state, based on their spectral characteristics. Low state sources were characterized by a powerlaw spectrum alone, whereas the high state sources required an additional multicolored disk component. Since the ULX in M31 is characterized by combination of a powerlaw and multicolored disk model, we place it in the category of "high" state ULXs. Therefore, we selected a reduced sample pertaining to "high" state ULXs, from Winter et al. (2006) sample of 32 galaxies. Moreover, we selected the brightest epoch out of multiple XMM-Newton observations, and those were not always available in Winter et al. (2006). Our final selection was limited to 19 sources with ULXs in "high" state and with brightest epoch observation, listed in Winter et al. (2006).

Figure 6. displays the resulting set of "high" state ULXs in the Luminosity - Temperature plane. As Winter et al. (2006) pointed out, the temperature distribution is possibly bimodal. The ULX in M31 belongs to the high-Temperature group, which is commonly believed to represent the stellar mass black holes. The low-Temperature group is characterized by a larger range of X-ray luminosities and has been tentatively attributed to the hypothetical class of IMBHs. The physical sample between low-T and high-T group is clearly visible, though the sample size is quite small. In this case, a different formation scenario can be attributed to these subsets of ULXs. The authors suggested that the one possibility is associated with the unique feature of pair-instability supernovae (PISNe) in the early universe (Population III origin, Heger et al. (2003).

The other comparison of ULXs in "high" state from this sample had been attributed to Temperature-Photon Index plane, as shown in Fig. 7. The low-T group displays a large range in photon index, resembling the large range in luminosity, however the uncertainties in the Photon Index parameter are quite large. In this figure,

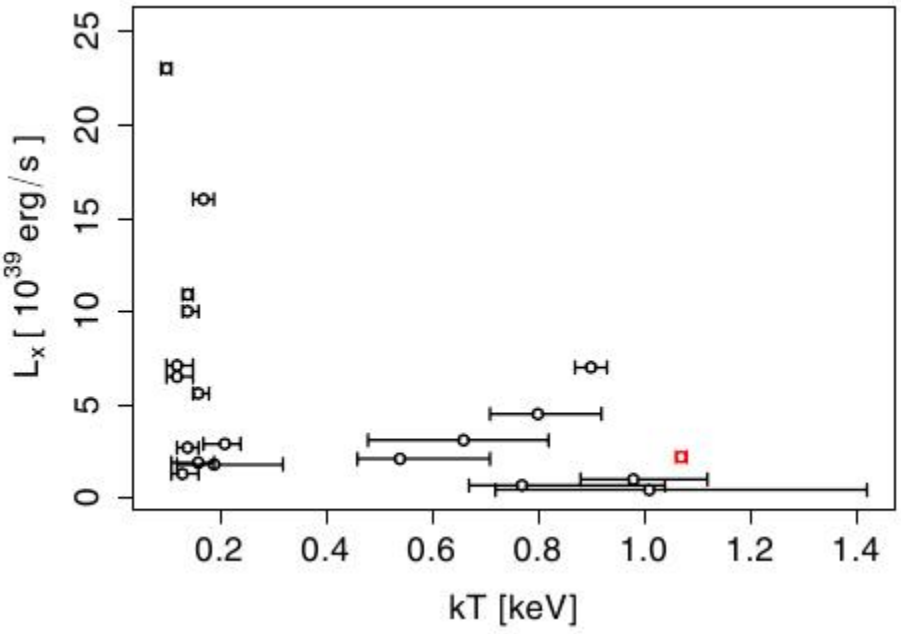

Figure 4.6 Temperature vs Luminosity for 19 selected ULXs from Winter et al. (2006) along with the candidate ULX (red) in M31. The M31 source is a member of the "high temperature" subgroup.

evolution of M31 ULX is shown, which shows a significant drop in temperature, but still retained in the high temperature regime. Referring back to Fig. 5, we noticed that over the period of observations with XMM-Newton, the source undergoes significant cooling leading to a drop in overall unabsorbed luminosity. But the individual thermal and non-thermal components did not exhibit the similar decline. The non-thermal component declined much rapidly as compared to the thermal component. The overall evolution of this source is thus a combination of a strongly varying thermal component and slightly varying non-thermal component.

We obtained the light curve for this ULX by combining all the data from Chandra, Swift and XMM-Newton. We deduce that the ULX X-ray luminosity follows an exponential decline (See Fig. 8) corresponding to a time constant $\sim$ 32 days. A

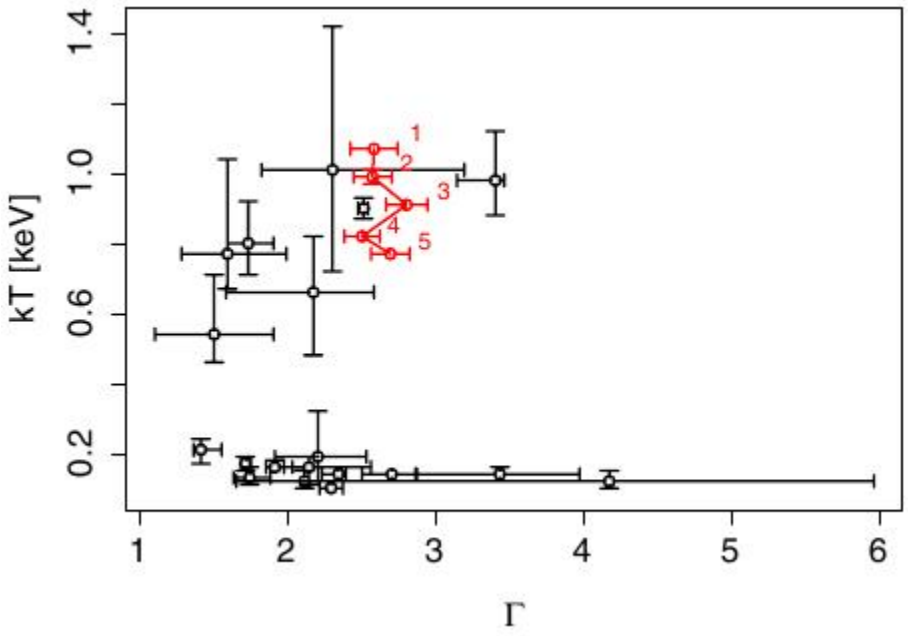

Figure 4.7 Photon Index vs Luminosity for 19 selected ULXs from Winter et al. (2006) along with the candidate ULX (red) in M31. The M31 source is a member of the "low photon index" subgroup.

continuation of this trend is evident from data taken 150 days after the outburst when the source was detected at $\sim 19^{38}$ erg/s (Barnard et al., 2005) . This observed exponential decline of the luminosity is consistent with galactic X-ray novae (Chen et al., 1997), which show FRED (Fast Rise Exponential Decay) like light curves. In our case, the FR part is missed. However, the light curves of this source class often exhibit more complex behavior than a simple exponential decay.

4.5 Summary

In summary, the Chandra discovery of ULX-1 in M31 established this source as the first ultraluminous source in M31. Follow up observations with Swift, XMM-Newton and Chandra revealed an exponential decline, reminiscent of the time evolu-

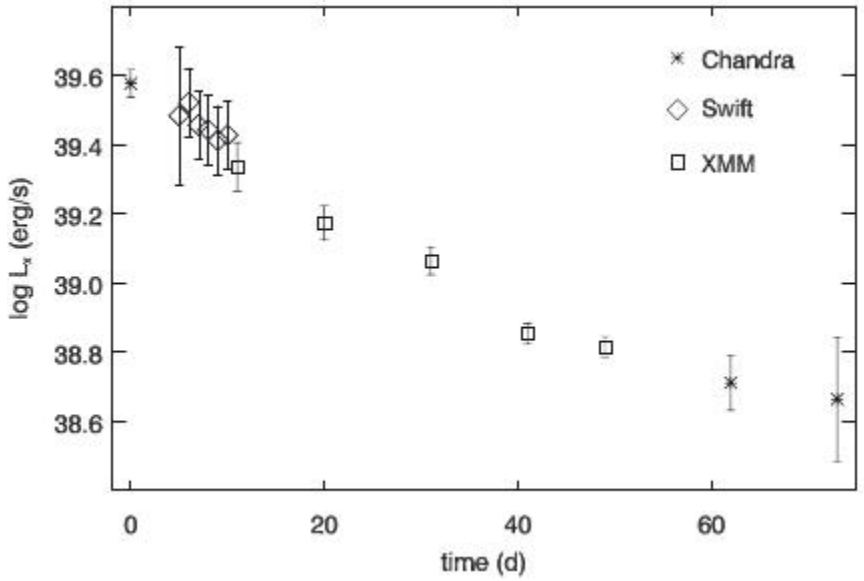

Figure 4.8 Variation of the total unabsorbed luminosity (L_{unabs}) of ULX in M 31 as observed by *Swift*−XRT, *Chandra* HRC-I and XMM−Newton resembling an exponential decay with a time scale of 32 days. The time zero corresponds to *Chandra HRC − I* observation ID 10886 (see table 1).

tion of Galactic X-ray novae. Spectral analysis of the XMM-Newton data suggest that this source was in a "high" state at the time of observation, and that the underlying source is likely a stellar mass black hole accreting near the Eddington limit.

4.6 Note on ULX-2

XMMU J004243.6+412519 (ULX-2) spectral analysis by Esposito et al. (2012) revealed a stellar mass black hole $\sim$ 12 $M_\odot$ as the underlying source. Based on the simple `DISKBB` model in `XSPEC`, the authors derived a maximum luminosity $\sim 1.1 \times 10^{39}$ erg/s. Additionally, a main sequence star with mass 8-10 $M_\odot$ or a giant with mass < 8 $M_\odot$ was suggested as the companion to the stellar mass black hole in the underlying binary system implying a high mass X-ray binary.

Chapter 5

Spatial Distribution of the Underlying Sources

It is discovered in chapter 4 that both the ULXs discovered in M31 contain Stellar Mass Black Holes (StMBH) as the primary compact component in the underlying binary system. Therefore, the scenario in these two cases seems to be more consistent with "StMBH accreting at Super-Eddington rate" model. Moreover, most of the optical counterpart studies reveal HXMBs (High Mass X-ray Binaries) as the underlying source, the recent observations by Soria et al. (2012) has raised an interesting possibility that the donor might be LMXBs (Low Mass X-ray Binaries), instead. We test the correlation of ULXs found in M31 with LMXBs and HMXBs, and therefore construct two 3-dimensional models based on spatial distribution of LMXBs and HMXBs in the galaxy.

5.1 LMXB Based Spatial Distribution Model

The galactic distribution of LXMBs is known to closely trace the stellar distribution, as one would expect similar to the old stars, would represent the older populations. To evaluate the spatial distribution of ULX sources, we therefore, use starlight as a proxy. A classic galactic decomposition would include a extended halo, a thin and a thick disk and a bulge/bar. To simplify this model, we focus on a double exponential disk model for M31. The disks of spiral galaxies are often modeled with a double exponential profile (Freeman, 1970). We construct a 3-dimensional Monte Carlo mass model of the disk of M31 to place the recently discovered ULXs in the context of their underlying populations. This model assumes a single source population following a double exponential distribution as follows:

$$exp^{-r/R_h} exp^{-z/H}$$

The scale length, R_h and scale height, H are fixed to 5.3 kpc and 100 pc, respectively as derived from Courteau et al. (2011). In this model, we assume a distance of M31 from the Sun = 785 kpc (Holland, 1998) and adopted the known values for inclination = 77deg and an arbitrary position angle. Our studies require surface brightness profiles, which do not change with the position angle, hence the position angle was kept arbitrary. The resulting 3-dimensional model is then projected on the sky which yields the spatial source distribution in the disk of M31 (Figure 1.) and then compared with the surface brightness profile of M31 (disk component only) obtained by Courteau et al. (2011). See Figure 2. We evaluate the surface brightness profile from our projected image of M31, as shown in Fig. 2, using task `ellipse` in `IRAF`. The detailed procedure is described in Appendix (chapter 7).

In general, a surface brightness profile traces stellar light in a galaxy, which is

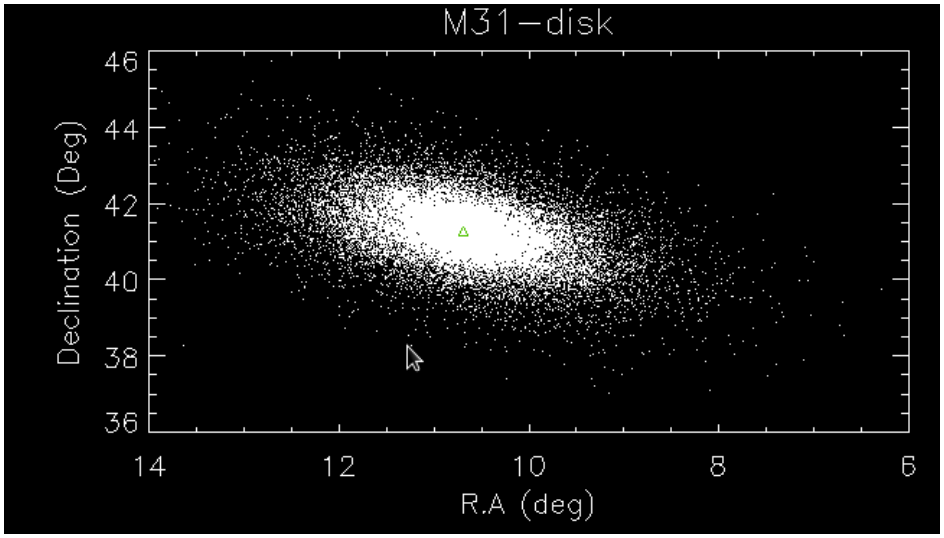

Figure 5.1 Right Ascension (degrees) and Declination (degrees) (on x-axis and y-axis, respectively) plot of projected M31 image on the sky.

followed by the X-ray source population distribution (Bogdán and Gilfanov, 2010). Bogdán and Gilfanov (2010) studied the brightness distribution of unresolved X-ray emission in M31 in the 0.5-7 keV energy range and established a strong correlation between the X-ray luminosity (L_x) and the K-band luminosity (L_K) as shown in Fig. 3. An approximately fixed ratio, L_x/L_K confirmed that the X-ray flux followed the near-infrared profile for M31, i.e. the stellar light profile.

Moreover, Swartz et al. (2011) explains that the ULX population distribution follows the stellar light. These authors conducted a statistical survey, based on 107 ULX candidates in a sample of 127 nearby galaxies in order to understand the underlying populations for ULX phenomenon. In this study, they concluded that the the surface distribution of ULXs in a galaxy follows a generalized exponential, similar to the De Vaucouleurs profile, $exp(f/h)^{1/n}$, n $\sim$ 3.6. This result is illustrated in Fig 4. The implication of this study revealed that the nature of the ULX population distribution is analogous to the stellar light distribution in a galaxy.

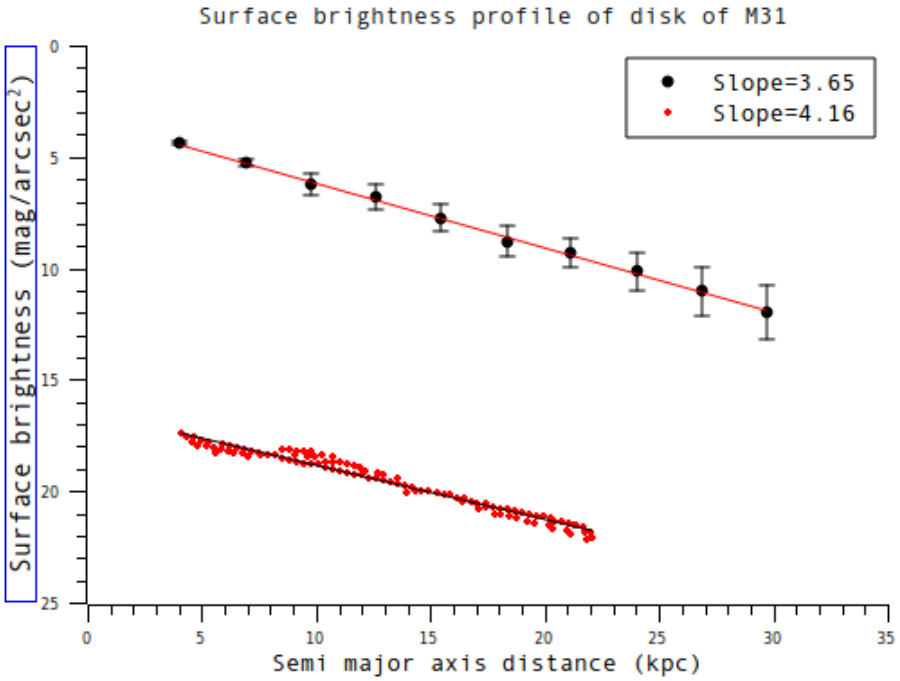

Figure 5.2 Surface brightness profile of the disk of M31 obtained from our spatial model of M31 with LMXBs and the M31 disk from Courteau et al. (2011). The surface brightness considered the bolometric magnitude of the Sun as the reference, whereas the Courteau et al. (2011)'s profile follows from 3.6 μm profile. The error bars in the figure represent the uncertainty in the average intensity along that isophote as generated by the *ellipse* task in `IRAF`.

Based on the disk model of M31, we calculate the radial probability distribution of ULXs found in M31. The simple disk model yields a small probability of 10% for finding a ULX within 2.3 kpc(spatial position of ULX-1). Therefore, an additional component i.e. bulge for this model is required. We modify our disk model of M31 to disk-bulge model of M31 based on the bulge to disk light ratio = 20% from Courteau et al. (2011). Addition of the necessary bulge component yields a better probability equal 21.2 % for a ULX to be found within 2.3 kpc from the center of M31. The radial probability distribution plots for ULXs derived from the disk only as well as the disk plus bulge model are shown below in Fig. 5 and Fig. 6. The two probability

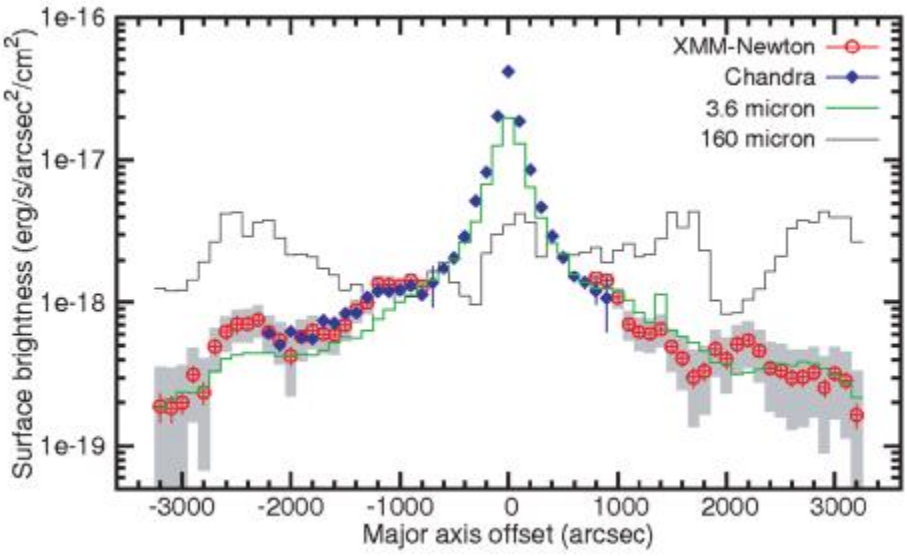

Figure 5.3 Surface brightness distribution for M31 in X-ray (blue, red) and infrared (grey, green) band. The shaded areas represent the uncertainty in the calculations for background subtraction for the XMM-Newton data.

values are derived based on the spatial location of ULX-1 and ULX-2.

The distribution functions yielded moderate probability for a ULX position based on two observations based on LMXB profile. Hence, this model does not overrule the possibility of LMXBs being the source population for ULXs, which was suggested by Soria et al. (2012). But, the HMXBs approach can not be overturned without testing the hypothesis for the latter. We discuss the correlation of ULXs with HMXBs in the next section.

5.2 HMXB Approach

As discussed in chapter 1, the optical observations of ULX counterparts often suggest the presence of massive stars, in these systems, which leads us to consider the class of high mass X-ray binaries as the underlying source population. The high mass

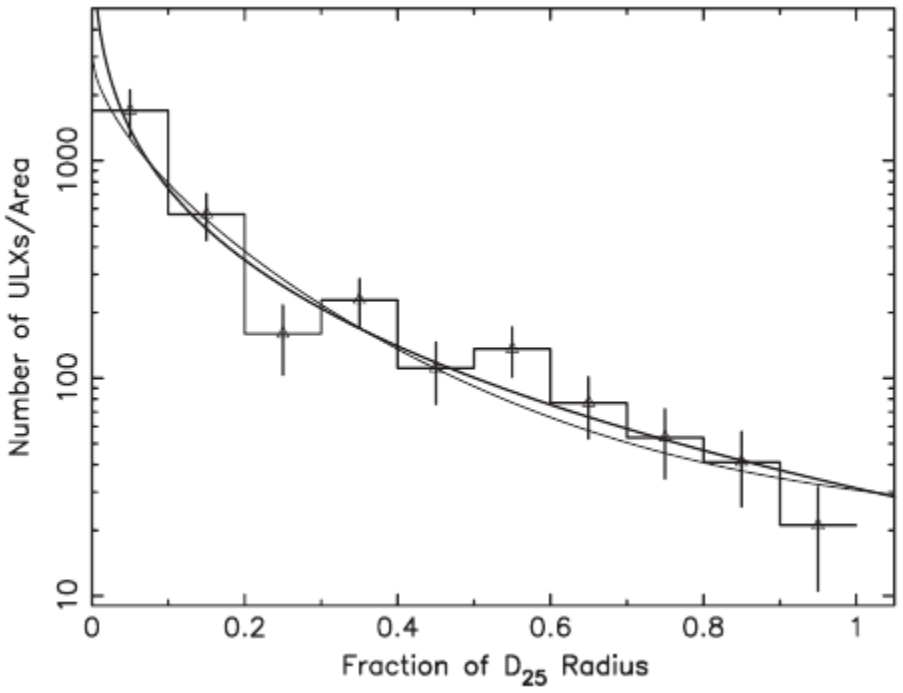

Figure 5.4 Surface distribution of ULX candidates. The abscissa is the radial position, expressed as a fraction of D_{25} radius. The ordinate is the number of ULX candidates per unit area *fdf* in the range *f* to *f* + *df*.

of the donor star (O and Be type) then implies that the overall age of the system is such that these sources should spatially trace recent star formations The global star formation patterns in galaxies can be traced in a variety of ways. See Kennicutt and Evans (2012) for the recent review. What is required for this study is a wide field of view image of M31, from which the location of star forming regions can be derived. Fig. 7 shows six commonly used tracers (Fritz et al., 2012) for which this data is available. The star forming regions are obviously seen in all these different observed bands. But, we select the tracer that provides the highest angular resolution and is free of confusion with diffused emission in inner part of M31. Therefore, we will focus on the Spitzer image 250 μm.

When this image is de-projected, i.e. M31 is rotated to yield a face on view,

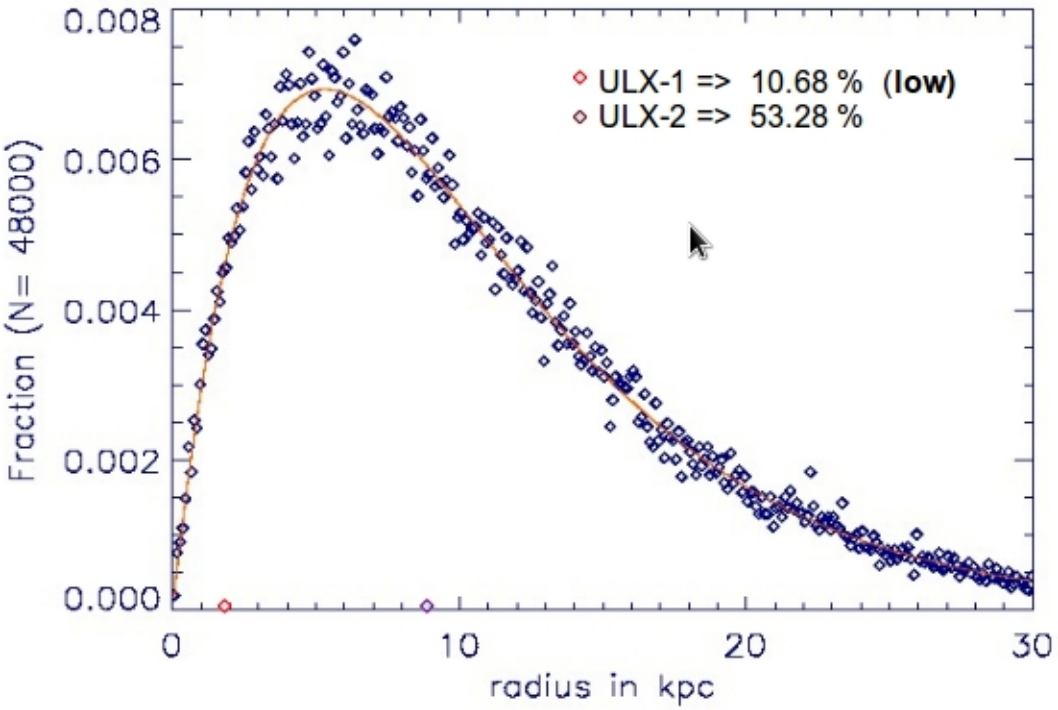

Figure 5.5 Radial probability distribution for the disk model. The abscissa is the distance away from the center of M31 and the ordinate represents the fraction of source population. The total number of sources is 48000.

these observations reveal a mixed ring like and spiral structure (Gordon et al., 2006). The dominant star forming structure is composed of two main rings at 10kpc and 15 kpc. An additional ring like structure appears inside of the 10 kpc ring. In addition to these rings, segments of spiral structure appear to be present.

To evaluate how ULX-1 and ULX-2 relate to the star forming signatures of M31, we show the actual Spitzer image in Fig. 8, which reveals that these source as well coincides with high surface brightness position at 250 μm. The innermost regions of M31 show a very complex star forming pattern, where neither rings nor spirals might be the appropriate geometric structures and even appearance of bar like

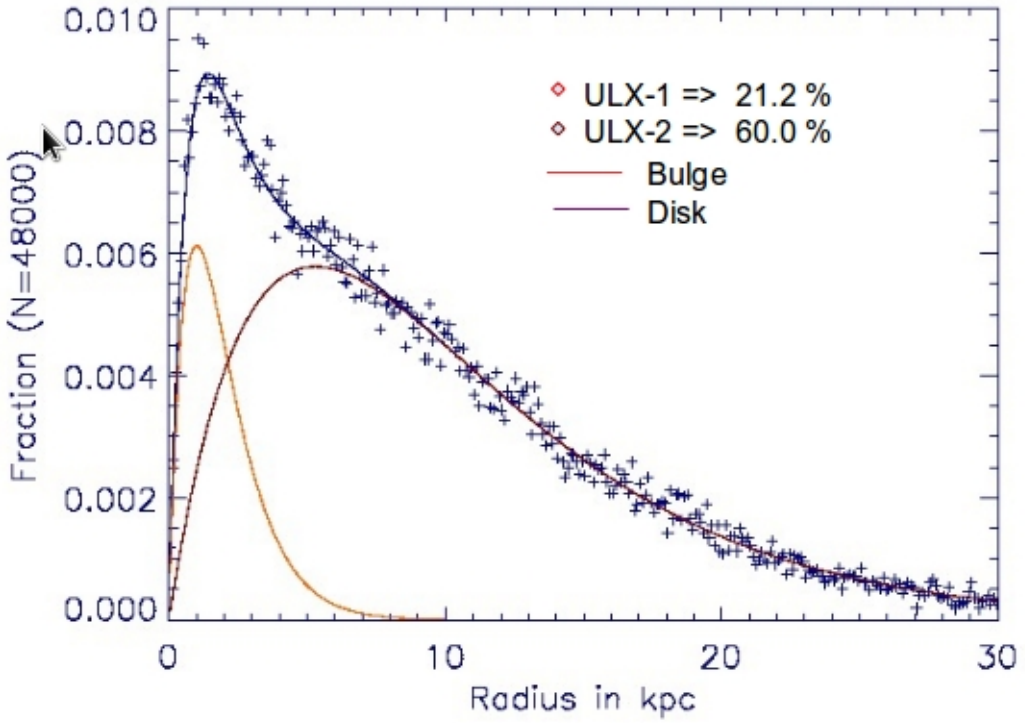

Figure 5.6 Radial probability distribution for the bulge in addition to the disk model.

features makes the task more complicated. Nonetheless, the coincidence with high surface brightness at 250 μm strongly argues for a connection with ULX-1 position and star forming activity. ULX-2 clearly coincides with one of the inner ring structure of M31.

The main issue addressed in this section is the spatial star formation tracer and its correlation with the ULX position. The exact identification of whether ULXs are in a specific arm/ring is not relevant for this work. The main concern is the correlation between star forming regions and position of ULXs. In contrast to the model, which is a Monte Carlo simulation on LXMB system, as discussed above, yields a small probability for a spatial coincidence with the inner arm of M31. The

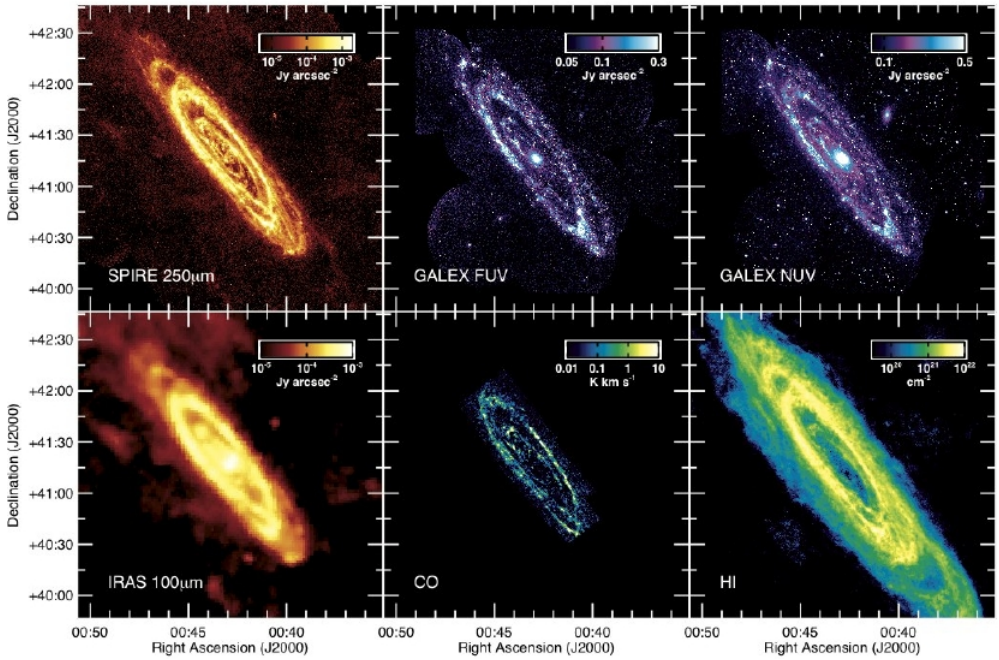

Figure 5.7 Surface brightness profiles of M31 shown in different wavelengths as shown in Fritz et al. (2012).

association of ULX sources with star formation galaxies is being studied in a recent study by Servillat et al. name, et al. 2012, a poster presented at " An INTEGRAL view of the high-energy sky (the first 10 years) - 9th INTEGRAL Workshop and celebration of the 10th anniversary of the launch", to be published by PoS, which analyzed Herschel data for ULX host galaxies.

Further implications of these studies are discussed in the next chapter.

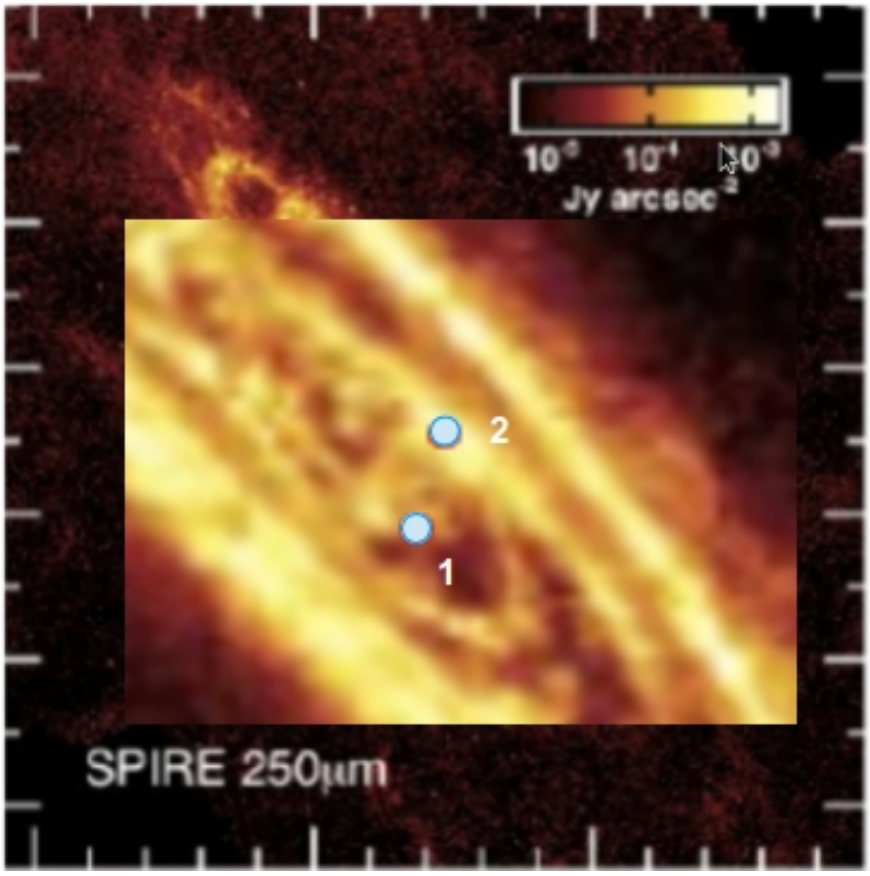

Figure 5.8 The blue dots overlapped on the zoomed Spitzer image of M31 derived from Fritz et al. (2012) represent the position of ULX-1 (*lower*) and ULX-2 *upper*.

Chapter 6

Conclusion and Discussion

Observations of Ultraluminous X-ray sources in nearby galaxies have implied X-ray binaries as their underlying source populations. The primary in the binary system is either a stellar mass black hole or possibly an intermediate mass black hole, and the companion (secondary) is either a high mass (O/Be type) star or a low mass A type star, which would correspond to a HMXB or LXMB system, respectively. Most observations of the optical counterparts revealed a "blue" star implying a younger massive star, but a recent observation of a ULX in M83 by Soria et al. (2012) arrived at a different result. The authors found a bright blue optical counterpart during the ULX phenomenon, but inspection of the previous images of M83 (a face on galaxy), revealed that the region of the ULX was found mainly populated with low mass stars. The absence of a "blue" star prior to the outburst lead the authors to propose a new theory of X-ray irradiation of a low mass companion during the ULX outburst, resulting in the increased brightness and the temperature and this is often observed as a blue counterpart during this process. Therefore, they suggested a LMXB association with ULXs rather than HXMBs. This model constitutes a major paradigm shift in this field, but it is thus far only based on a single source. In contrast, ongoing study

of host galaxies of ULXs by Servillat et al. name, et al. 2012, a poster presented at " An INTEGRAL view of the high-energy sky (the first 10 years) - 9th INTEGRAL Workshop and celebration of the 10th anniversary of the launch", to be published by PoS suggests a link between star formation and the ULX positions. These authors selected 20 host galaxies at a distance < 40 Mpc, from catalogs established by Swartz et al. (2011), Sutton et al. (2012), Gladstone et al. (2009) and compared the observed position of each ULX with the *Herschel-PACS* image. The association of ULXs with star forming regions in their host galaxies e.g. IC342, M81, M101 and Holmberg II was very apparent. Moreover, in most of these spiral galaxies, ULXs were found in the outer spiral arm structures.

We constrain the nature of ULX-1 and ULX-2 discovered in M31 in 2009 and 2012, respectively based on observational and theoretical studies. We found that the ULX-1 and ULX-2 in M31 host a stellar mass black hole with $M_{BH} \sim 13$ $M_{\odot}$ (see chapter 4) and ~ 10 $M_{\odot}$ (Esposito et al., 2012). This evidence aligns well with the near-Eddington accretion theory for stellar mass black holes and argues against the involvement of an intermediate mass black hole.

The association of ULXs with LXMBs has been studied via population modeling explained in chapter 5. Based on our simple model of M31 (a double exponential disk plus a similar bulge model), we conclude that the ULX positions are consistent with the distribution of light, which correlates with the distribution of LMXBs (Bogdán and Gilfanov, 2010). The association of ULXs with HMXBs is examined with simple inspection of IR images from Spitzer (Fritz et al., 2012). The ULX-2 is found to coincide with one of the inner star forming structures located within the 10 kpc star forming. The ULX-1 is very close to the nucleus of M31, which makes it difficult to analyze its correlation or anti-correlation with star formation regions. Superimposing

the position of this ULX on the 250μm Spitzer image from Fritz et al. (2012) yields a clear association with star forming activity (traced by 250μm emission). The fact that the both ULXs in M31 correlate with star forming regions suggests a likely association of ULXs with HMXBs.

Moreover, as mentioned above, the ULXs in most of the nearby spiral galaxies are found in their outer spiral arm structures, while the ULXs in M31 are located relatively near the nucleus and appear to correlate with the inner spiral structure. To explain this deviation between inner and outer positions, we point out that the ULXs found in M31 were discovered by a nova monitoring program in the inner regions of M31 (See Fig. 1.) using XMM-Newton and Chandra. This selection bias may be

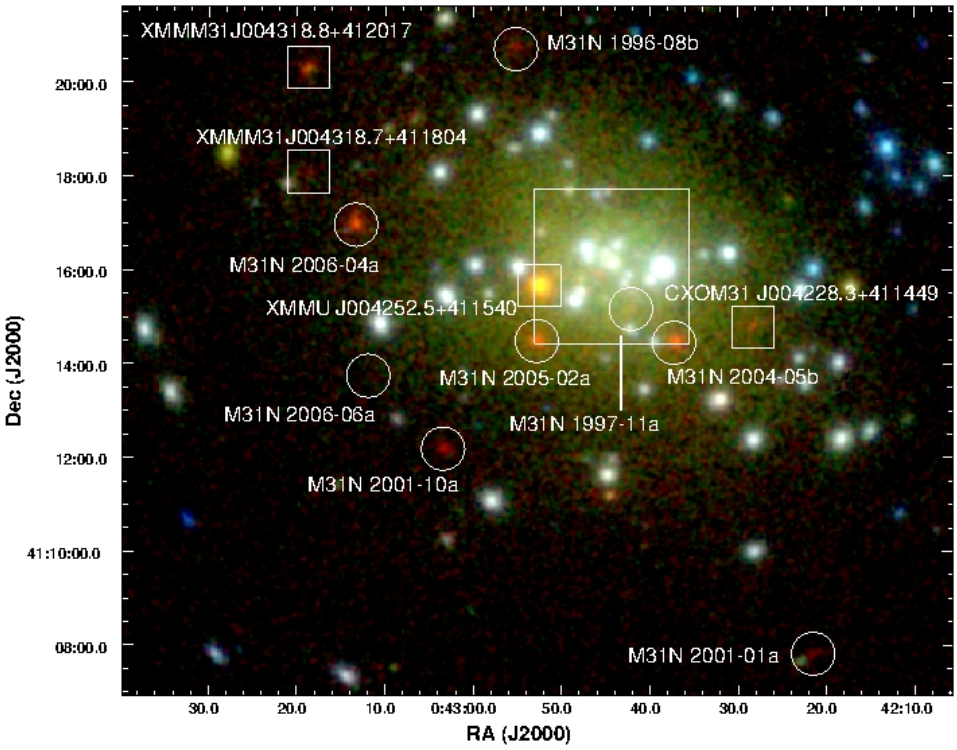

Figure 6.1 XMM-Newton EPIC -pn, MOS1, MOS2 combined image from Henze et al. (2010) illustrating the field of view of M31 for the nova monitoring program.

overcome with future wide field of view X-ray surveys that would be able to monitor

the galaxies as large as M31 (> 2 deg), possibly resulting in further discoveries of ULXs in M31. Our own galaxy has so far no ULX source, while M31 only recently acquired two members of this class. With very few exceptions (antennae) such small numbers appear to be the norm to investigate whether or not the ULX frequency per galaxy may be used as a tracer for the star formation rate, deserves the further investigation.

Appendices

Appendix A

XMM-Newton Data Analysis with SAS

An example of XMM-Newton spectral reduction and analysis is demonstrated in this chapter usingSAS[1]. We obtained spectra of CXOM31 J004253.1+414222 utilizing all three European Photon Imaging Cameras (`EPIC`) `pn, MOS1` and `MOS2`. The data obtained from `HEASARC` [2] are processed through a pipeline `epchain` for `pn`, `emchain` for `MOS1/MOS2` utilizing the software `SAS`. The resultant event file is used to create image, spectra and light curve shown in Fig 1, 2 and 3, respectively.

The spectrum is obtained with the task `evselect` by extracting the source region (circular, in general) with X and Y sky center coordinates and radius in pixels, from the image obtained from the event file. A `PATTERN` value less than 4 and 12 are used to reduce the noise level for `pn` and `MOS1/MOS2`, respectively. Also, `FLAG` is set to zero value in order to avoid the bad pixels.

[1] http://xmm.esac.esa.int/sas/

[2] *http : //heasarc.gsfc.nasa.gov/docs/xmm/xmmhp_archive.html*

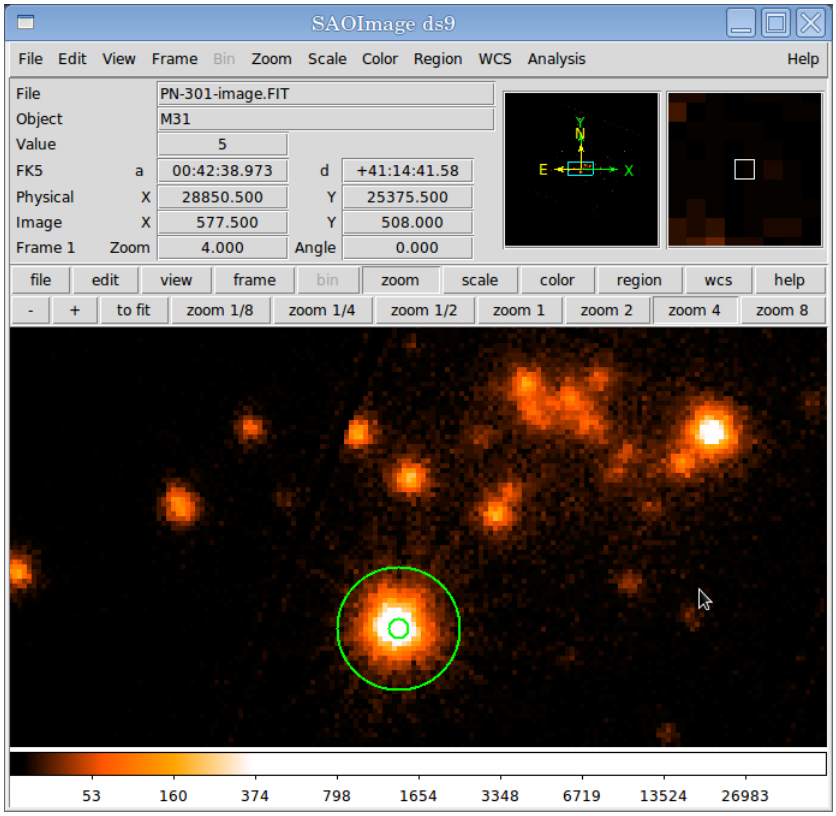

Figure A.1 An example EPIC-pn image from XMM-Newton for ID 0600220201

Pile up correction

To estimate the amount of pile up, `epatplot` is used. Fig 7.4 displays an example spectra with pile-up problem. The pile up is clearly shown as a deviation of obtained spectra from the model spectra. In order to correct the spectra from pile up, an annulus region is used for the source extraction using `DS9`, instead of a circular region. The inner circle region is considered the piled up data and is discarded for the process of spectrum extraction. This test is performed with the task, `epatplot` e.g. in Fig 4, which is pile up corrected spectrum from Fig 5. An annular *background* spectrum is also obtained around the source extraction region.

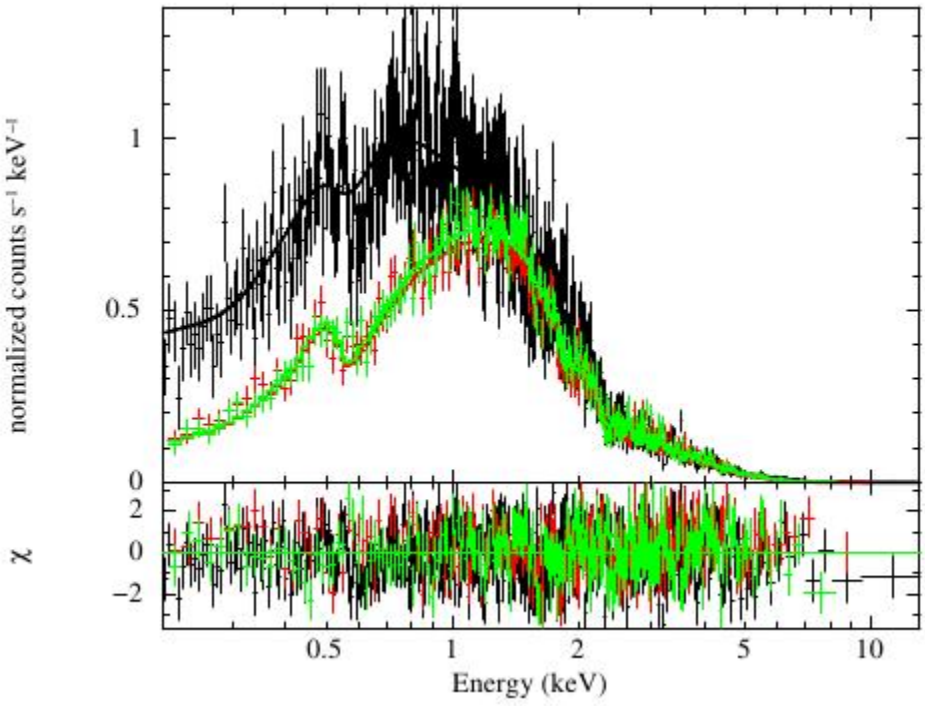

Figure A.2 An example spectra for EPIC-pn for ID 0600220201 obtained with XMM-Newton

The light curve is obtained with a time binning of 100s using the task `evselect` and `FLAG` value set to zero to reject bad pixels.

An Ancillary Response file `ARF` and Redistributed Matrix File `RMF` are obtained with `arfgen` and `rmfgen`, respectively. These files and the background spectrum are grouped with the source spectrum, which then is binned to obtain atleast the minimum number of counts per bin using `GRPPHA`. The grouped source spectrum is then read into `XSPEC` for spectral fitting. The bad pixels are ignored and the only energy levels between 0.2 keV - 10keV are accepted for analysis.

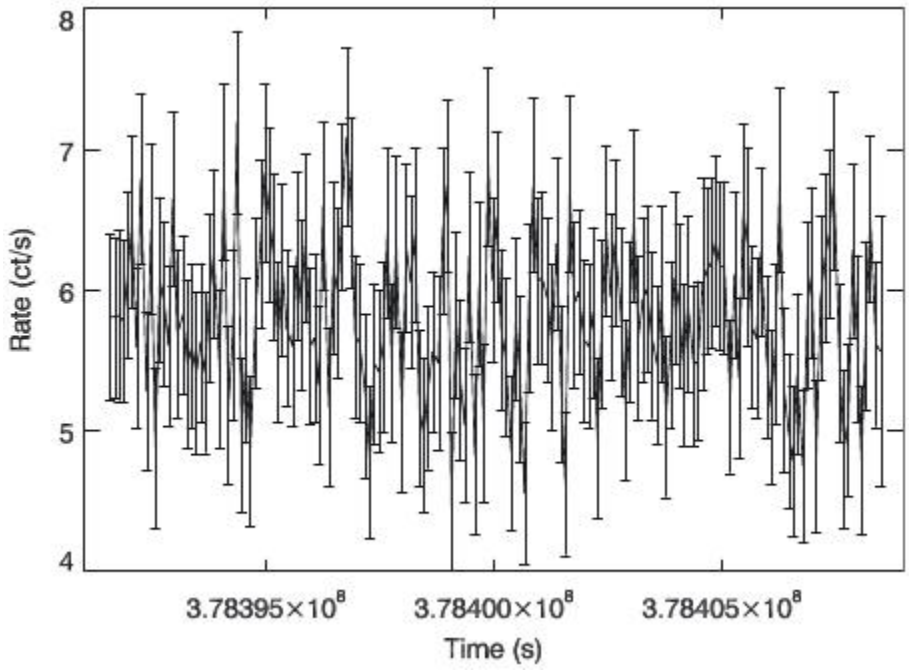

Figure A.3 XMM-Newton light curve for ID 0600220201 with time binning of 100s in 0.2-10keV

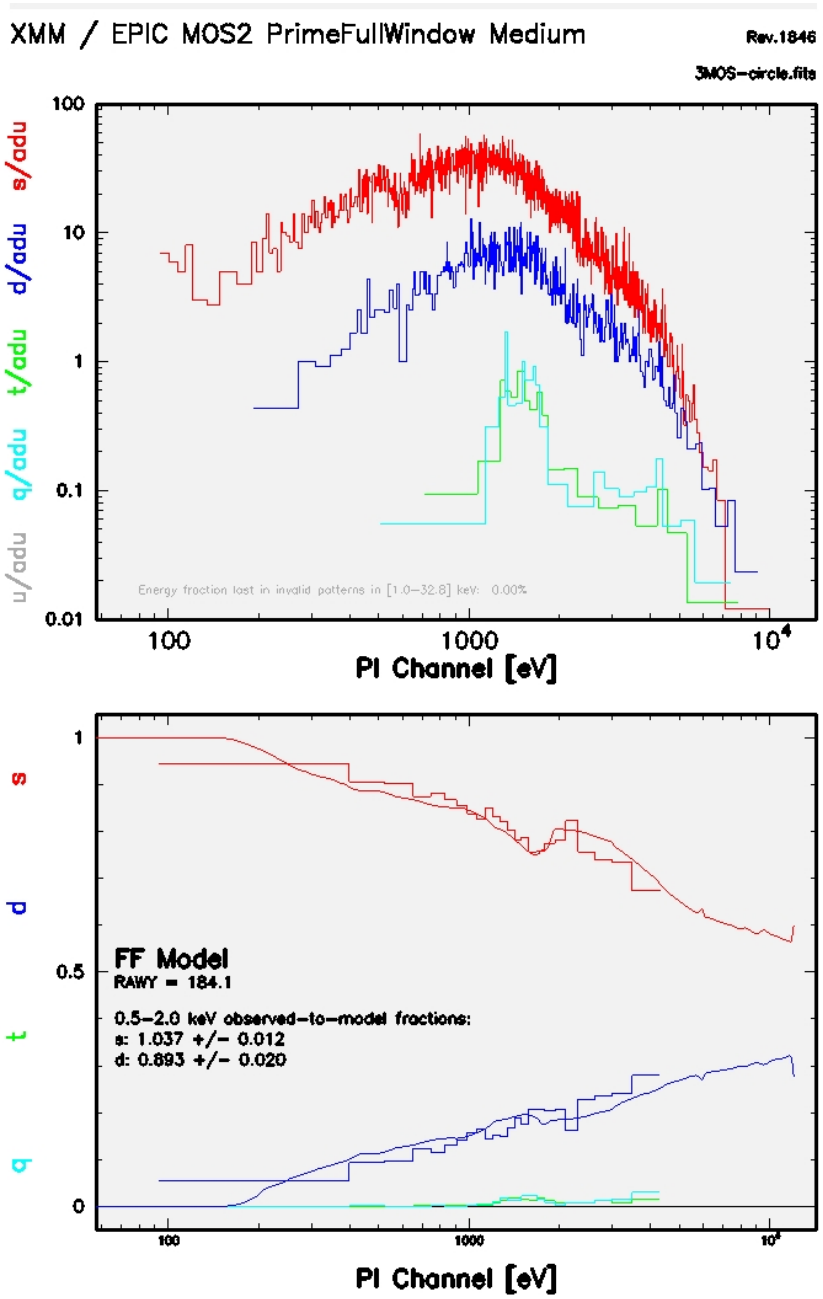

Figure A.4 The model fit to the observed PSF for our source. The upper panel displays the spectra of Singles, doubles, triples and quadruples events in red, blue, green and light blue, respectively. The lower panel displays the fraction of all these events at varied energy levels. Clearly the count level for doubles from our source exceed the model curve.

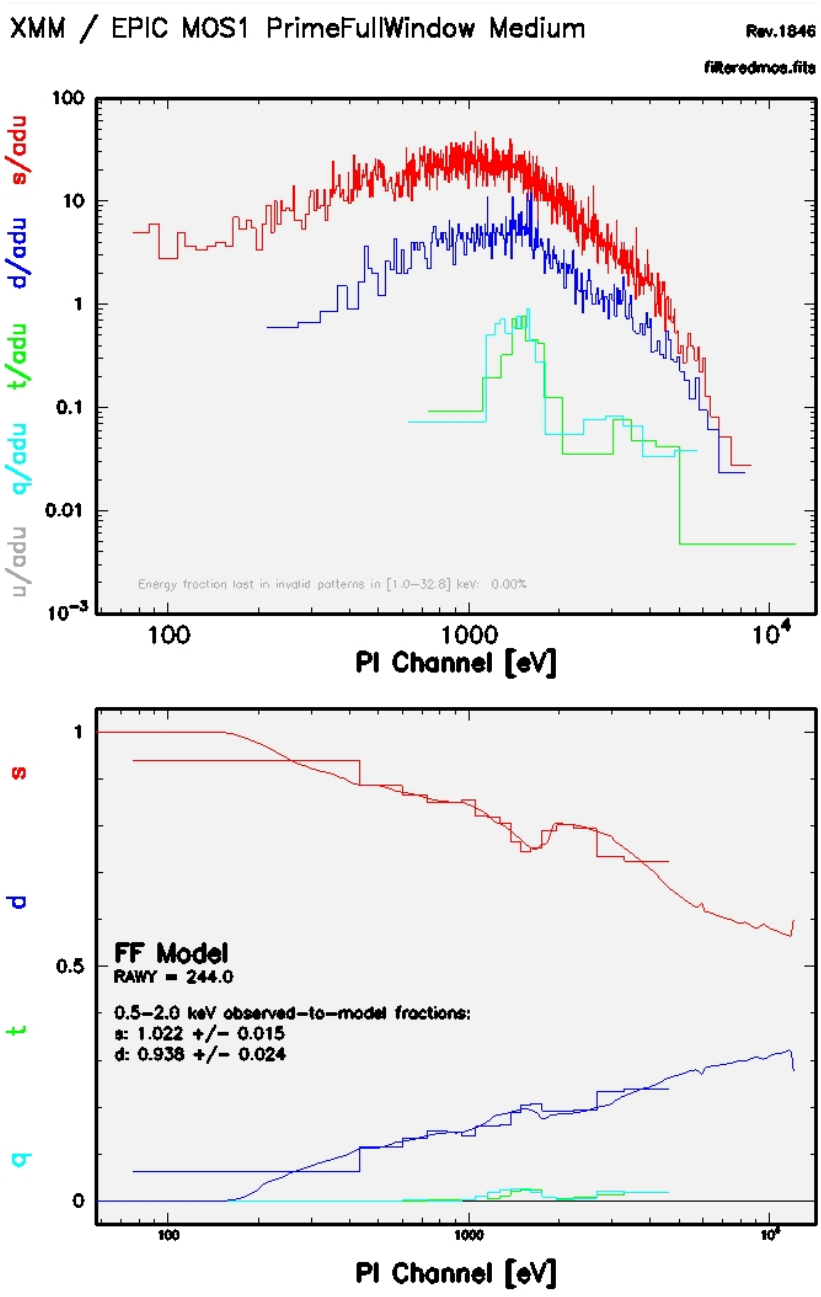

Figure A.5 The pile up corrected observed source fit to the model. The pile up correction yielded the overlap of our data with the model curve.

Appendix B

IRAF- surface brightness

To evaluate the surface brightness profile from the projected view of 3-dimensional M31 disk model, we used `IRAF` version 2.14.1. First of all, the projected image of M31 was converted into an eqivalent CCD image with dimension 512 $\times$ 512. The task `ellipse` from `IRAF` was employed to generate the elliptical isophotes of constant "Intensity, (I)(counts /pixel)" along the semi-major axis of M31. The center of M31 obtained from the 3D model, was fixed during this task, while the eccentricity and position angle were free parameters. This task utilizes the method described in Jedrzejewski,RobertI. (1987) to estimate the these isophotes. The counts per pixels are then converted to "surface brightness, μ" (mag/arcsec^2) considering the Sun as a reference with apparent bolometric magnitude, $m_\odot$ (m_{ref} below) =-26.74. The following formulae were employed for this conversion:

$$m - m_{ref} = -2.5\ log_{10}\left(\frac{f}{f_{ref}}\right)$$

$$\mu = m + 2.5\ log_{10}(\Omega)$$

The model assumes 10^{11} stars with mass, M = 1 $M_{\odot}$ in Andromeda galaxy. f_{ref}, is the bolometric flux of the Sun = 1.376 $\times 10^{6}$ erg $s^{-1}cm^{2}$. Flux along an isophote of given intensity, I is $f = \left(\frac{L_{isophote}}{4\pi D_{M31}^{2}}\right)$. $L_{isophote}$= number of stars along the isophote $\times$ the bolometric luminosity of the Sun. Ω is the solid angle corresponding to a single pixel, in $arcsec^{2}$.

Bibliography

Abramowicz, M. A., Czerny, B., Lasota, J. P., and Szuszkiewicz, E. (1988). Slim accretion disks. *The Astrophysical Journal*, 332:646.

Abramowicz, M. A., Jaroszyski, M., Kato, S., Lasota, J.-P., Róaska, A., and Sdowski, A. (2010). Leaving the innermost stable circular orbit: the inner edge of a black-hole accretion disk at various luminosities. *Astronomy and Astrophysics*, 521:A15.

Banerji, M., McMahon, R. G., Hewett, P. C., Alaghband-Zadeh, S., Gonzalez-Solares, E., and Venemans, B. P. (2012). Heavily Reddened Quasars at z˜2 in the UKIDSS Large Area Survey: A Transitional Phase in AGN Evolution. page 18.

Barnard, R., Greening, L. S., Tonkin, C., Kolb, U., and Osborne, J. P. (2005). XMM-Newton reveals 100 new LMXBs in M31 from variability studies. (230):119–122.

Begelman, M. C. (2001). SuperEddington Atmospheres That Do Not Blow Away. *The Astrophysical Journal*, 551(2):897–906.

Begelman, M. C. (2002). Super-Eddington Fluxes from Thin Accretion Disks? *The Astrophysical Journal*, 568(2):L97–L100.

Belczynski, K., Bulik, T., Fryer, C. L., Ruiter, A., Valsecchi, F., Vink, J. S., and Hurley, J. R. (2010). on the Maximum Mass of Stellar Black Holes. *The Astrophysical Journal*, 714(2):1217–1226.

Bogdán, A. and Gilfanov, M. (2010). Unresolved X-ray emission in M31 and constraints on progenitors of classical novae. *Monthly Notices of the Royal Astronomical Society*, 218:209–218.

Caballero-García, M. D. and Fabian, A. C. (2010). X-ray reflection in a sample of X-ray bright ultraluminous X-ray sources. *Monthly Notices of the Royal Astronomical Society*, 402(4):2559–2566.

Chen, W., Shrader, C. R., and Livio, M. (1997). The properties of x-ray and optical light curves of x-ray novae 1. pages 1–68.

Colbert, E. J. M., Mushotzky, R. F., Reynolds, M., and Matteo, D. (1999). THE NATURE OF ACCRETING BLACK HOLES IN NEARBY GALAXY NUCLEI We have found compact X-ray sources in the center of 21 (54 %) of 39 nearby face-on spiral and ellip- tical galaxies with available ROSAT HRI data . ROSAT X-ray luminosities (0 . 2È2 . 4 keV) . 1.

Colbert, E. J. M. and Ptak, A. F. (2002). A Catalog of Candidate IntermediateLuminosity XRay Objects. *The Astrophysical Journal Supplement Series*, 143(1):25–45.

Coppi,P.S. (2000). EQPAIR: A Hybrid Thermal/Non-Thermal Model for the Spectra of X-Ray Binaries. *American Astronomical Society*, 32.

Courteau, S., Widrow, L. M., McDonald, M., Guhathakurta, P., Gilbert, K. M., Zhu, Y., Beaton, R. L., and Majewski, S. R. (2011). THE LUMINOSITY PROFILE AND STRUCTURAL PARAMETERS OF THE ANDROMEDA GALAXY. *The Astrophysical Journal*, 739(1):20.

Dewangan, G. C., Miyaji, T., Griffiths, R. E., and Lehmann, I. (2004). A Transition to a Low/Soft State in the Ultraluminous Compact X-Ray Source Holmberg II X-1. *The Astrophysical Journal*, 608(1):L57–L60.

Dickey, J. M. and Lockman, F. J. (1990). H I in the Galaxy. *Annual Review of Astronomy and Astrophysics*, 28(1):215–259.

Done, C. and Kubota, A. (2006). Disccorona energetics in the very high state of Galactic black holes. *Monthly Notices of the Royal Astronomical Society*, 371(3):1216–1230.

Ebisawa,Ken, ycki,Piotr, Kubota,Aya, Mizuno,Tsunefumi, and Watarai,Ken-Ya (2003). Accretion Disk Spectra of the Ultra-luminous X-ray Sources in Nearby Spiral Galaxies and Galactic Superluminal Jet Sources. *Chinese Journal of Astronomy & Astrophysics*, 3:415–424.

Esposito, P., Motta, S. E., Pintore, F., Zampieri, L., and Tomasella, L. (2012). Swift observations of the ultraluminous X-ray source. 9(October):1–9.

Fabbiano, G. (1989). X Rays From Normal Galaxies. *Annual Review of Astronomy and Astrophysics*, 27(1):87–138.

Fabian, A. C., Ross, R. R., and Miller, J. M. (2004). On the observed disc temperature of accreting intermediate mass black holes. *Monthly Notices of the Royal Astronomical Society*, 355(2):359–362.

Fabian,A.C. and Ward,M.J. (1993). ROSAT PSPC Observations of the Extragalactic HII Region NGC5408. *Monthly Notices of the Royal Astronomical Society*, 263.

Freeman, K. C. (1970). On the Disks of Spiral and so Galaxies. *The Astrophysical Journal*, 160:811.

Fritz, J., Gentile, G., Smith, M. W. L., Gear, W. K., Braun, R., Roman Duval, J., Bendo, G. J., Baes, M., Eales, S. A., Verstappen, J., Blommaert, J. A. D. L., Boquien, M., Boselli, A., Clements, D., Cooray, A. R., Cortese, L., De Looze, I., Ford, G. P., Galliano, F., Gomez, H. L., Gordon, K. D., Lebouteiller, V., OHalloran, B., Kirk, J., Madden, S. C., Page, M. J., Remy, A., Roussel, H., Spinoglio, L., Thilker, D., Vaccari, M., Wilson, C. D., and Waelkens, C. (2012). The Herschel Exploitation of Local Galaxy Andromeda (HELGA). *Astronomy & Astrophysics*, 546:A34.

Fryer, C. L. (1999). Mass Limits For Black Hole Formation. *The Astrophysical Journal*, 522(1):413–418.

Gammie, C. F. (1998). Photon bubbles in accretion discs. *Monthly Notices of the Royal Astronomical Society*, 297(3):929–935.

Garcia,M., Murray,S., Primini,F., Callanan,P., and Nooraee,N. (2010). Optical ID of CXOM31 J004253.1+411422, a bright Black Hole X-ray Nova in M31. *The Astronomer's Telegram*.

Gladstone, C., Roberts, T. P., and Done, C. (2009). The Ultraluminous State . 17(May):1–17.

Gladstone, J., Roberts, T., and Done, C. (2011). Unlocking the nature of ultraluminous X-ray sources using their X-ray spectra. *Astronomische Nachrichten*, 332(4):345–348.

Gordon, K. D., Bailin, J., Engelbracht, C. W., Rieke, G. H., Misselt, K. A., Latter, W. B., Young, E. T., Ashby, M. L. N., Barmby, P., Gibson, B. K., Hines, D. C., Hinz, J., Krause, O., Levine, D. A., Marleau, F. R., Noriega-Crespo, A., Stolovy, S., Thilker, D. A., and Werner, M. W. (2006). Sp i t zer MIPS Infrared Imaging of M31: Further Evidence for a Spiral-Ring Composite Structure. *The Astrophysical Journal*, 638(2):L87–L92.

Heger, A., Fryer, C. L., Woosley, S. E., Langer, N., and Hartmann, D. H. (2003). How Massive Single Stars End Their Life. *The Astrophysical Journal*, 591(1):288–300.

Henze, M., Pietsch, W., Haberl, F., Hernanz, M., Sala, G., Della Valle, M., Hatzidimitriou, D., Rau, A., Hartmann, D. H., Greiner, J., Burwitz, V., and Fliri, J. (2010). X-ray monitoring of classical novae in the central region of M31. *Astronomy & Astrophysics*, 523:A89.

Henze,M., Pietsch,W., Haberl,F., and Greiner,J. (2009). CXOM31 J004253.1+411422 - a very bright new X-ray transient in M 31 discovered with Chandra and Swift. *The Astronomer's Telegram*.

Henze,M., Pietsch,W., Haberl,F., and XMM-Newton/ChandraM31NovaMonitoringCollaboration (2012). XMMU J004243.6+412519 - a new X-ray transient in M 31 seen with XMM-Newton. *The Astronomer's Telegram*.

Holland, S. (1998). The Distance to the M31 Globular Cluster System. *The Astronomical Journal*, 115(5):1916–1920.

Jedrzejewski,RobertI. (1987). CCD surface photometry of elliptical galaxies. I - Observations, reduction and results. *Monthly Notices of the Royal Astronomical Society (ISSN 0035-8711)*, 226:747–768.

Kaaret, P. (2002). A Chandra High Resolution Camera Observation of XRay Point Sources in M31. *The Astrophysical Journal*, 578(1):114–125.

Kaur, a., Henze, M., Haberl, F., Pietsch, W., Greiner, J., Rau, a., Hartmann, D. H., Sala, G., and Hernanz, M. (2012). CXOM31J004253.1+411422: the first ultraluminous X-ray transient in M31. *Astronomy & Astrophysics*, 538:A49.

Kennicutt, R. C. and Evans, N. J. (2012). Star Formation in the Milky Way and Nearby Galaxies. *Annual Review of Astronomy and Astrophysics*, 50(1):531–608.

King, A. R., Davies, M. B., Ward, M. J., Fabbiano, G., and Elvis, M. (2001). Ultraluminous X-Ray Sources in External Galaxies. *The Astrophysical Journal*, 552(2):L109–L112.

Madau, P. and Rees, M. J. (2001). Massive Black Holes as Population III Remnants. *The Astrophysical Journal*, 551(1):L27–L30.

Makishima, K., Kubota, A., Mizuno, T., Ohnishi, T., Tashiro, M., Aruga, Y., Asai, K., Dotani, T., Mitsuda, K., Ueda, Y., Uno, S., Yamaoka, K., Ebisawa, K., Kohmura, Y., and Okada, K. (2000). The Nature of Ultraluminous Compact XRay Sources in Nearby Spiral Galaxies. *The Astrophysical Journal*, 535(2):632–643.

Marchant, A. B. and Shapiro, S. L. (1980). Star clusters containing massive, central black holes. III - Evolution calculations. *The Astrophysical Journal*, 239:685.

Miller, J. M., Fabian, A. C., and Miller, M. C. (2004). A Comparison of Intermediate-Mass Black Hole Candidate Ultraluminous X-Ray Sources and Stellar-Mass Black Holes. *The Astrophysical Journal*, 614(2):L117–L120.

Miller, M. and Colbert, E. J. M. (2004). INTERMEDIATE-MASS BLACK HOLES. *International Journal of Modern Physics D*, 13(01):1–64.

Miller, M. and Hamilton, D. P. (2002). Production of intermediate-mass black holes in globular clusters. *Monthly Notices of the Royal Astronomical Society*, 330(1):232–240.

Miller, N. A., Mushotzky, R. F., and Neff, S. G. (2005). Radio Emission Associated with the Ultraluminous X-Ray Source in Holmberg II. *The Astrophysical Journal*, 623(2):L109–L112.

Mitsuda,K., Inoue,H., Koyama,K., Makishima,K., Matsuoka,M., Ogawara,Y., Suzuki,K., Tanaka,Y., Shibazaki,N., and Hirano,T. (1984). Energy spectra of low-mass binary X-ray sources observed from TENMA. *Astronomical Society of Japan*, 36:741–759.

Nooraee, N., Callanan, P. J., Barnard, R., Garcia, M. R., Murray, S. S., and Moss, a. (2012). Chandra , Swift , and HST studies of the CXOM31 J004253.1+411422. *Astronomy & Astrophysics*, 542:A120.

Quinlan, G. D. and Shapiro, S. L. (1990). The dynamical evolution of dense star clusters in galactic nuclei. *The Astrophysical Journal*, 356:483.

Roberts, T. P., Warwick, R. S., Ward, M. J., Goad, M. R., and Jenkins, L. P. (2005). XMM-Newton EPIC observations of the ultraluminous X-ray source NGC 5204 X-1. *Monthly Notices of the Royal Astronomical Society*, 357(4):1363–1369.

Ross, R. R. and Fabian, A. C. (2005). A comprehensive range of X-ray ionized-reflection models. *Monthly Notices of the Royal Astronomical Society*, 358(1):211–216.

Shakura,N.I. and Sunyaev,R.A. (1973). Black holes in binary systems. Observational appearance. *Astronomy and Astrophysics*, 24.

Soria, R., Kuntz, K. D., Winkler, P. F., Blair, W. P., Long, K. S., Plucinsky, P. P., and Whitmore, B. C. (2012). THE BIRTH OF AN ULTRALUMINOUS X-RAY SOURCE IN M83. *The Astrophysical Journal*, 750(2):152.

Stobbart, A.-M., Roberts, T. P., and Wilms, J. (2006). XMM-Newton observations of the brightest ultraluminous X-ray sources. *Monthly Notices of the Royal Astronomical Society*, 368(1):060323074251006–???

Supper, ., Hasinger, ., Pietsch, ., Truemper, ., Jain, ., Magnier, ., Lewin, ., and vanParadijs, . (1997). ROSAT PSPC survey of M 31. *Astronomy and Astrophysics*.

Sutton, A. D., Roberts, T. P., Walton, D. J., Gladstone, J. C., Scott, A. E., and Mar, H. E. (2012). The most extreme ultraluminous X-ray sources : evidence for intermediate-mass black holes ? 26(March):1–26.

Swartz, D. A., Ghosh, K. K., Tennant, A. F., and Wu, K. (2004). THE ULTRALUMINOUS X-RAY SOURCE POPULATION FROM THE CHANDRA ARCHIVE OF GALAXIES. pages 519–539.

Swartz, D. A., Soria, R., Tennant, A. F., and Yukita, M. (2011). A COMPLETE SAMPLE OF ULTRALUMINOUS X-RAY SOURCE HOST GALAXIES. *The Astrophysical Journal*, 49(1):49.

Titarchuk, L. (1994). Generalized Comptonization models and application to the recent high-energy observations. *The Astrophysical Journal*, 434:570.

vanParadijs,J. and McClintock,J.E. (1995). Optical and ultraviolet observations of X-ray binaries. *X-ray binaries*.

Walton, D. J., Gladstone, J. C., Roberts, T. P., and Fabian, A. C. (2010). A Large Catalogue of Ultraluminous X-ray Source Candidates in Nearby Galaxies. page 4.

Webb, N., Cseh, D., Lenc, E., Godet, O., Barret, D., Corbel, S., Farrell, S., Fender, R., Gehrels, N., and Heywood, I. (2012). Radio detections during two state transitions of the intermediate-mass black hole HLX-1. *Science (New York, N.Y.)*, 337(6094):554–6.

Williams, B. F., Naik, S., Garcia, M. R., and Callanan, P. J. (2006). A Catalog of Transient XRay Sources in M31. *The Astrophysical Journal*, 643(1):356–375.

Wilms, J., Allen, A., and McCray, R. (2000). On the Absorption of XRays in the Interstellar Medium. *The Astrophysical Journal*, 542(2):914–924.

Winter, L. M., Mushotzky, R. F., and Reynolds, C. S. (2006). XMMNewton Archival Study of the Ultraluminous XRay Population in Nearby Galaxies. *The Astrophysical Journal*, 649(2):730–752.

Zwart, S. F. P., Baumgardt, H., Hut, P., Makino, J., and McMillan, S. L. W. (2004). Formation of massive black holes through runaway collisions in dense young star clusters. *Nature*, 428(6984):724–6.

Zwart, S. F. P., McMillan, S. L. W., Hut, P., and Makino, J. (2001). Star cluster ecology - IV. Dissection of an open star cluster: photometry. *Monthly Notices of the Royal Astronomical Society*, 321(2):199–226.